Up-scaling High Harmonic Generation in capillary waveguides based on increasing capillary diameter

Florian Sterl Ale Strooisma

December 15, 2011

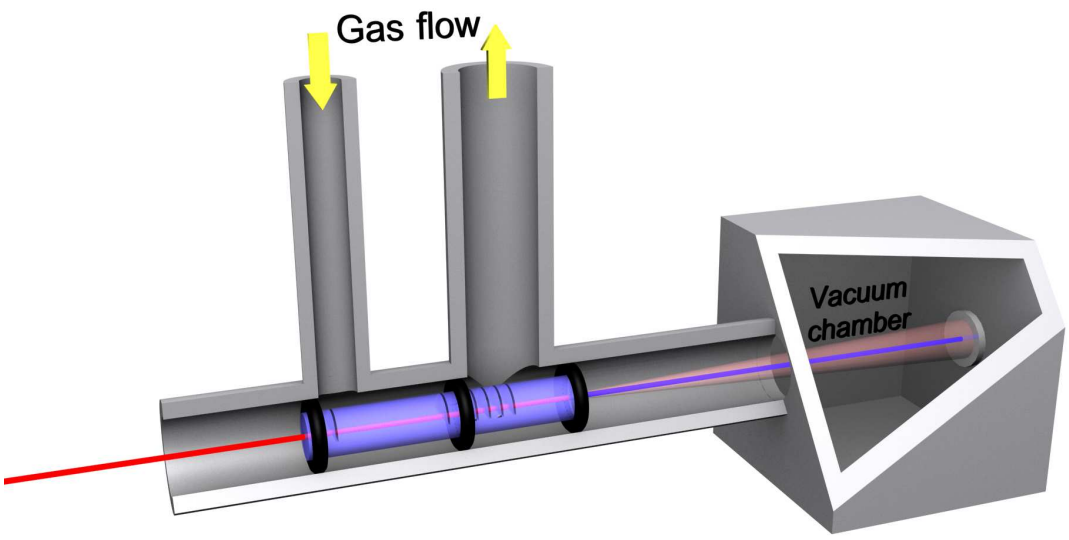

Abstract

The optical properties of EUV free-electron lasers can be improved by seeding the laser. Capillary waveguide based high-order harmonic generation (HHG) sources have shown to provide the required beam quality for seeding such lasers: ultrashort pulses of coherent light with extremely short wavelengths. Traditionally those systems cannot produce the high pulse energy required for seeding an FEL. Therefore, experimental research is conducted in increasing the capillary diameter to increase high harmonic power output. However, as the diameter is increased, gas load onto the UHV undulator of the FEL grows problematically. Also, the particle density and thus the EUV absorption behind the capillary is increased, reducing the power output. The solution of differential pumping via slits in the capillary wall is investigated in this report via experiments as well as a theoretical study and numerical analysis.

Nomenclature

Latin Letters

C	flow conductivity	Ls^{-1}
D	diameter	m
F	force	N
f	friction factor	
Δk	phase mismatch	
L	length	m
N	atomic density	m^{-3}
n	harmonic order	
p	pressure	$mbar$
$\bar{p}$	mean pressure	$mbar$
Δp	pressure difference	$mbar$
Q	volume flow rate	Ls^{-1}
q	particle flowrate	$mbarLs^{-1}$
Re	Reynolds number	
S	pumping speed	m
t	time	s
u	velocity	ms^{-1}
V	volume	L

Greek Letters

α	absorption coefficient	
γ	specific heat ratio	
μ	dynamic viscosity	$kgm^{-1}s^{-1}$
ρ	mass density	kgm^{-3}
σ	absorption cross section	m^2
τ	shear stress	Pa

Contents

Chapter 1

Introduction

This research is part of a project performed in collaboration with FERMI@Elettra, a single-pass free-electron laser user facility located in Trieste, Italy. This FEL operates in the wavelength range from 10 to 100 nanometer.

A Free Electron Laser (FEL) is a laser device, which can generate femtosecond pulses with ultrahigh intensities at wavelengths tunable in a wide range down to a few nanometers, using oscillating free electrons. Those pulses can be used to investigate the dynamics of processes at atomic scale with very high temporal resolution. A major problem with a FEL is that it starts from noise and output is generated in a single pass. Consequently the pulse energy strongly fluctuates and the FEL has a short coherence length and varying spectrum. However, this can be improved by seeding the FEL with a coherent XUV beam.

However, in the XUV wavelength region it is difficult to realize laser sources, because a much higher input power is needed to reach lasing threshold, since the threshold increases inversely with λ^5, where λ is the laser wavelength. Also, in this wavelength range most materials are highly absorptive and it is hard to make efficient transmitting mirrors, which limits XUV laser oscillators to double pass. However, coherent XUV light can be generated by sources based on High Harmonic Generation (HHG) in gases and may therefore provide a suitable seeding source. Coherent XUV generation based on HHG is demonstrated down to 0.35 nm. [9]

HHG is an extreme nonlinear frequency conversion process where an ultrahigh intensity laser beam is focused into a gas, generating a broad spectrum of odd harmonics. In order to generate a high output over a long interaction length, the gas is inserted into a capillary that guides the drive laser beam. The XUV beam is transported through vacuum towards diagnostics and the FEL to prevent absorption.

In currently existing set-ups, however, the intensity of the generated wave is not high enough to be useful for seeding an FEL. In order to increase the produced intensity, increasing the intensity of the input wave has been proposed; however, this does not work, since a higher intensity input wave will ionize the gas, hence disturbing the effect of HHG. Another approach consists of increasing the diameter of the used capillary. In that case more energy can be applied over a larger area, thus increasing the total output energy without affecting the input intensity.

Increasing the diameter, however, puts forward a new problem: a larger diameter means a larger gas flow. Since the capillary is open on both ends this means a large increase of gas flowing into the vacuum system. This flow can easily become so large that the pressure in the vacuum system gets so high that absorption of the generated harmonics becomes severe. Another problem that occurs is that the gas load on the FEL becomes too high. A solution for these problems is to apply differential pumping between the part of the capillary where HHG is done and the end of the capillary.

In order to construct a capillary pumping system, extra length has to be added to the capillary in order to accommodate gas outlet slits and thus achieve the required pressure gradient inside the capillary instead of behind it. This report investigates the influence of factors like this extra capillary length, capillary diameter and number of outlet slits on minimum achievable vacuum pressure. It will also try to make predictions about the best method to increase the output power in HHG.

The report is organized as follows: In Chapter 2, the FEL, the principle of HHG and the proposed methods of scaling the output of the HH source, and the gas flow theory needed to describe the flow through the capillary, are explained into further detail. Next in Chapter 3, flow rate measurements and differential pumping experiments are described. The results and simulations are reported in Chapter 4, followed by discussion in Chapter 5. Also conclusions will be drawn in Chapter 5. Finally in Chapter 6 recommendations for further research will be given.

Chapter 2

Theoretical background

The goal of the SeedFEL project is to scale up the output energy of the High Harmonic (HH) seeding source for the free-electron laser FERMI@Elettra. This chapter briefly describes relevant concepts and theories. First, the concept of the free-electron laser will be described. Next, an overview of the principles of high harmonic generation will be given as well as a description of a high harmonic source based on a gas-filled capillary waveguide. Finally, the flow theory required to describe the gas flows in the capillary waveguide will be discussed.

2.1 Free-electron Laser

A Free Electron Laser is a type of laser in which the kinetic energy of electrons moving at nearly light speed is transformed into coherent electromagnetic radiation. For this, an electron beam generated at a photocathode is accelerated in a linear accelerator up to GeV energy(figure 2.1). The electrons are injected into an undulator which comprises an array of alternatingly poled magnets producing a static and spatially sinusoidal magnetic field. Due to the Lorenz force, the electrons move in a sinusoidal trajectory in the reference frame of the undulator. However,in the reference frame of the electron beam (moving at the speed of the electrons), each electron is oscillating in the transverse direction, thus forming a dipole emitting synchrotron radiation. Yet, the problem is that the electrons enter the undulator at random moments in time, so they oscillate with a random phase such that the emitted radiation is incoherent.

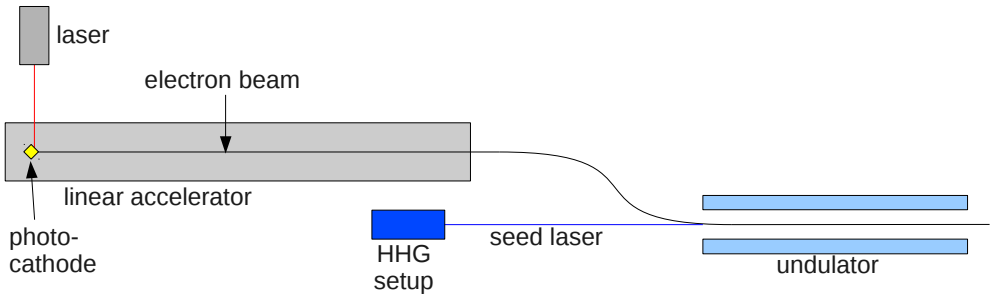

Figure 2.1: *The set-up of a Free Elecron Laser, seeded by a high harmonic source.*

This problem can be solved by applying a coherent seed beam to the electron beam, in order to make the electrons bunch together. Forces on the electrons resulting from the combined undulator and seed radiation field cause the electrons to bunch at the radiation wavelength, allowing a coherent

interaction between the electrons and the radiation. This force is called the ponderomotive force. The principle of the bunching is illustrated in Figure 2.2. In the region where the force of the laser beam is positive, the electrons are accellerated, whereas the electrons in the region with a negative force are decelerated, so that the electrons are 'trapped' in bunches separated by a distance of one wavelength of the electromagnetic field. Because the electrons are now distributed approximately periodically in bunches along the undulator, they oscillate - approximately - in phase, such that the emitted waves are in phase as well. The period of the undulator field is approximately equal to the period of the emitted wave, so the waves of all bunches are in phase as well, resulting in a coherent wave. [10]

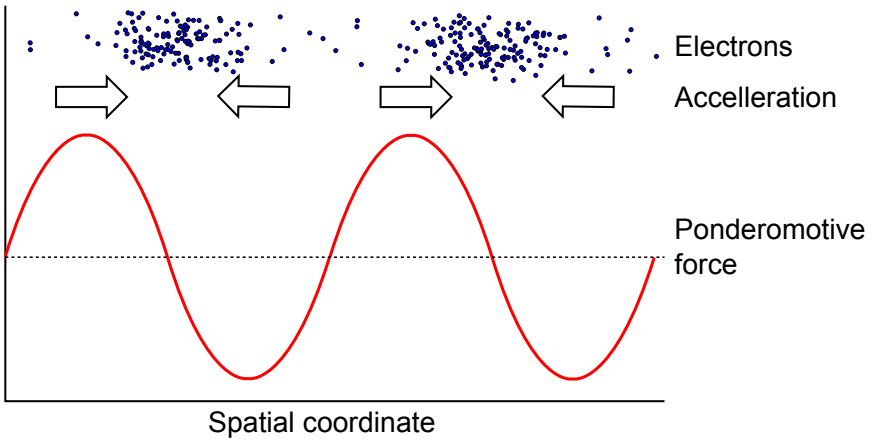

Figure 2.2: *The principle of bunching: a seeding laser beam is applied to the electron beam, forcing the electrons into bunches seperated by a distance of one wavelength. The horizontal axis is the spatial coordinate in a frame which moves with the speed of the electrons.*

2.2 High Harmonic Generation

For the seeding of FERMI@Ellettra, a coherent radiation source covering the wavelength regime from 30 to 100 nm (XUV) is required. Laser sources operating in this regime are not suitable for seeding because they generate only radiation at a single fixed wavelength. Sources based on HHG, however, form an attractive alternative as they produce a broad spectrum of odd multiples of the drive laser frequency extending into the XUV and soft-x-ray range.

High harmonics can be generated by focusing an intense laser pulse into a gas jet. To explain the process of HHG a semi-classical model can be used that comprises three steps illustrated in figure 2.3. In this model, the outer electron of each gas atom is considered to be in the potential well created by the atom. In the first step, a strong external electric field, such as produced by a short laser pulse, is applied that tilts the potential well (figure 2.3a: step1) thereby lowering the barrier and enabling tunnel ionization of the electron. In the second step, after the tunnel ionization, the electron behaves as a free particle in the laser field. The laser field accelerates the electron away from its ion until the second half of the optical cycle is reached and the field flips direction (figure 2.3b: step 2). Then the electron is accelerated back to the ion and with a certain probability recombines (figure 2.3c: step 3). In the last step, upon recombination, the kinetic energy of the electron is converted into radiation consisting of a broad range of odd harmonics of the drive laser frequency. The high harmonic spectrum may include up to hundreds of orders and extend well into the soft x-ray regime. The maximum photon energy that can be obtained is determined by the sum of the ionization potential of the atom and the kinetic energy of the electron. For efficient high harmonic generation, the drive laser and the generated harmonics have to be phase matched.

In the HH seed source for FERMI@Elettra, the drive laser will be focused into a capillary waveguide filled with a noble gas. A schematic of the seed source is shown in figure 2.4. The capillary is mounted

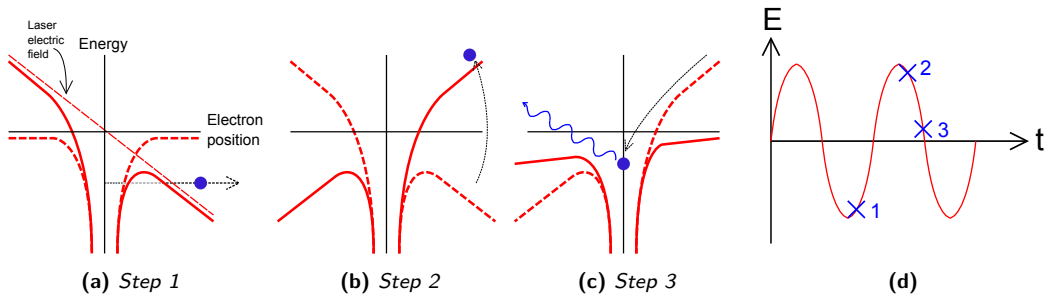

Figure 2.3: *Electron recollision model for HHG, comprising tunnel ionization of an electron (a), its acceleration in the drive laser field (b) and recombination of the electron with the parent ion (c). The three steps in the recollision model correspond to various phases of the driving field (d). (Adapted from [3])*

inside a tube that can be pumped vacuum to prevent absorption of the generated high harmonics in air. In the capillary wall, two inlet slits are cut that allow the gas to flow into the capillary, thus creating a region of constant pressure between the slits. Because the capillary is open at both ends, the gas will flow out there. Unfortunately, the capillary cannot be sealed with optical windows. Any window at the entrance of the capillary, were the drive laser is coupled in, would break due to the high intensity of the focused laser beam. Therefore, the vacuum tube holding the capillary is sealed with a window far before the focus of the laser. At the rear end, the capillary cannot be closed because a window would absorb the generated harmonics. Using vacuum tubing, the capillary can be connected downstream to a XUV spectrometer to measure the high harmonic spectrum or to the FEL for seeding experiments.

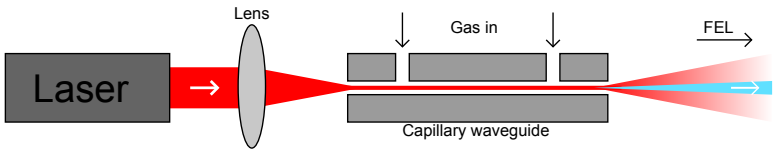

Figure 2.4: *A schematic of the high harmonic seed source. An infrared drive laser pulse is focused into a capillary waveguide. The capillary is filled with a gas from which high harmonic radiation is generated.*

2.2.1 Phase matching

To obtain a considerable amount of output the radiation emitted by all the individual atoms has to be in phase, such that the responses of the individual atoms add up to a macroscopic effect. However, a difference between the phase velocities of the drive laser radiation and the generated XUV radiation gives rise to phase mismatch (see figure 2.5).

If this phase matching is not achieved, the interaction length is limited to the coherence length of the conversion process, since at lengths larger than this length, the phase shift is π radians and thus the generation starts to interfere destructively. The coherence length, however, is usually much less than the intended interaction length.

Phase matching is achieved when the so-called *phase mismatch* is equal to zero. The phase mismatch can be derived from the wave equation for the fundamental laser radiation and the generated higher harmonics:

$$E_n = e^{i(k_n x - n\omega t)} \tag{2.1}$$

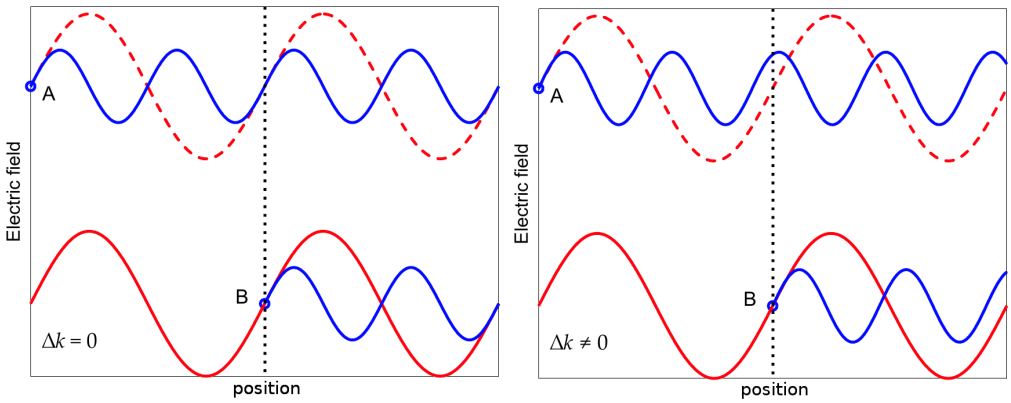

Figure 2.5: *Phase-matching of harmonic generation. (a) When the fundamental drive wave (red line) and second harmonic (blue line) propagate with the same phase velocity, the harmonics from points A and B add in phase, enhancing the signal; (b) when their phase velocities differ, the harmonics from A and B destructively interfere, decreasing the harmonic signal. Adapted from [2].*

where k_n is the wavevector of the generated radiation and q represents the harmonic order. The first harmonic order ($n = 1$) corresponds to the fundamental laser radiation (wavevector k_1).

The phase mismatch for each harmonic order is given by equation 2.2:

$$\Delta k = k_n - nk_1 = 0 \tag{2.2}$$

The phase mismatch depends on various parameters, namely the neutral gas dispersion, the plasma dispersion arising from the generation of free electrons and a factor determined by the waveguide The total phase mismatch is then given by (according to [2]):

$$\Delta k \approx n\frac{u_{11}^2\lambda_0}{\pi D^2} + N_e r_e(n\lambda_0 - \lambda_n) - \frac{2\pi N_a}{4\lambda_n}[\delta\lambda_0 - \delta(\lambda_n)], \tag{2.3}$$

in which N_a is the number density of neutral atoms and N_e is the number density of electrons, which both scale linearly with the gas pressure. $\delta\lambda_1 - \delta(\lambda_n)$ is the neutral gas dispersion at 1 bar, r_e is the classical electron radius and λ_n is the harmonic wavelength. Furthermore, u_{11} is the first zero of the Bessel function J_0 and a is the capillary radius.

From equation 2.3 it can be seen that phase matching can be achieved by tuning the gas particle density. This can easily be done inside a capillary waveguide by tuning the gas pressure.

2.2.2 High Harmonics absorption

If radiation is sent through gas, there will always be some absorption, regardless of the radiation frequency. How much of it is absorbed, however, is frequency-dependent. A measure for the amount of radiation which is absorbed while travelling through a certain length of gas is the so-called *absorption cross section* σ, measured in units of m^2, which is commonly expressed as:

$$\sigma = \frac{\alpha}{N}, \tag{2.4}$$

where α is the absorption coefficient (m^{-1}) and N is the atomic density of the gas (m^{-3}). From the absorption cross section, the amount of radiation transmitted through the gas can be calculated using the Lambert-Beer law:

$$\frac{I(L)}{I_0} = e^{-\int_0^L \sigma N(z)dz}, \tag{2.5}$$

where z is the path over which the radiation travels through the gas, over a length L. Figure 2.6a shows the absorption cross section as a function of the radiation frequency for argon, and figure 2.6b shows the transmission coefficient I/I_0 as a function of the pressure (which is directly related to the atomic density via the ideal gas law) at a wavelength of 50 nm, over a distance of 1 m (which is a realistic value for the length of the section before the radiation enters the ultra-high vacuum (almost non-absorbing) part of the FEL beam line). The figure shows that little radiation is absorbed for pressures of up to 10^{-4} mbar, but for higher pressures, the loss increases significantly.

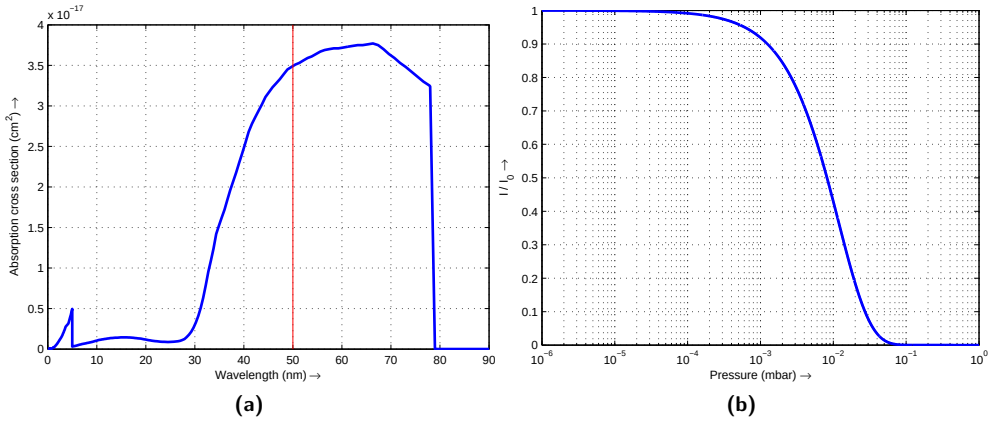

Figure 2.6: *Plot of absorption cross section versus wavelength for argon gas (a) (data were taken from [1]) and plot of transmission coefficient versus pressure for the absorption cross section at a wavelength of 50 nm, over a distance of 1 m (b).*

2.2.3 Scaling of HHG output power

As mentioned before, the interaction length of the noble gas inside the capillary, and thus the output power, is limited by the coherence length of the conversion process, but also by the absorption of the high harmonics by the gas. Thus, to increase the maximum output power, other methods have to be found. Technically it would be possible to increase the intensity of the drive laser, and thus the total input power, but this is also limited, since at too high levels of ionization, the laser light is defocused inside the capillary, inducing high energy losses. Furthermore, since the number density of electrons N_e (see equation 2.3 is increased and thus disturbes the phase matching. As soon as these two points have been optimized, the only remaining way of increasing the output power is increasing the input power without changing the input intensity, in other words, increasing the diameter of the input laser beam and thus the capillary diameter.

In this case however, a new problem arises. The flow through the capillary increases with the fourth power of the diameter as will be explained in section 2.3.3. This means that increasing the capillary diameter to increase output induces a large gas flow out of the capillary. This has two undesirable implications. First, the increased gas flow leads to a higher particle density in the section behind the capillary. This leads to a significantly larger absorption, again reducing the output power. Second, the gas flow out of the capillary leads to a large gas load toward the undulator of the FEL. The FEL can only operate at very low pressure, which becomes very hard to maintain if the gas load from the HHG source becomes large.

The solution to this problem, which is investigated throughout this report, is a novel differential pumping system integrated into the HHG source. Figure 2.7 schematically how this system is implemented. The source comprises a holder for the capillary with gas in- and outlet tubes. In the holder, the capillary is mounted using rubber o-rings for vacuum sealing. In the capillary wall behind the section with the inlet slits, multiple slits are made to allow gas flowing out of the capillary. The rings

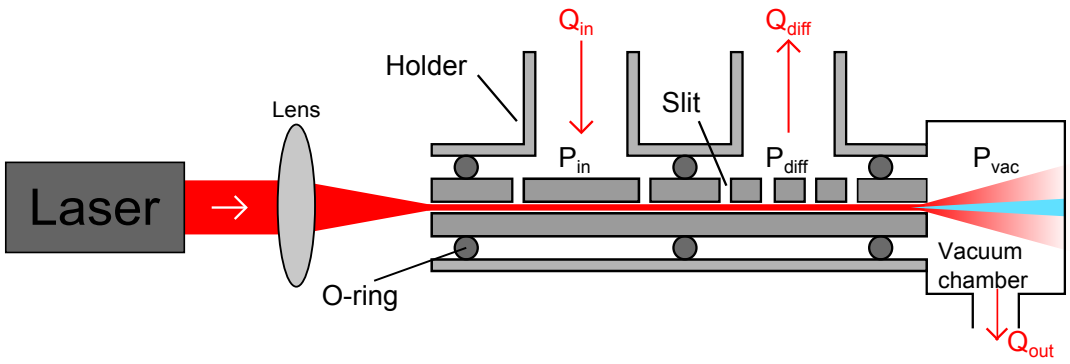

Figure 2.7: *Schematic overview of an HHG capillary inside a specially designed holder (longitudinal section). The gas enters the capillary via the first perpendicular tube and the first two slits (Q_{in}), and a portion of the gas exits the capillary via four other slits and the second perpendicular tube (Q_{diff}). The rubber o-rings separate the inlet slits and the outlet slits from each other and from the vacuum chamber.*

are placed such that the leftmost two slits (the inlet slits) can communicate with the left tube and the other slits with the right tube. The capillary is still open at both ends.

Gas is inserted into the capillary through the left tube at a constant rate, thus creating a region of constant pressure between the two leftmost slits. The part of the capillary after that is the differential pumping section, as explained in section 2.3.3. Gas is pumped out of the capillary here through the right tube. The vacuum chamber behind the capillary is evacuated to a very low pressure to prevent absorption of the generated harmonics.

There is one advantage of increasing the diameter of the capillary: from equation 2.3 is can be seen that, if the capillary diameter is increased, the pressure required to provide a phase mismatch of zero decreases. This effect is less strong than the increasing of the gas flow at bigger capillary diameters, but still, it is very practical: decreasing the pressure in the capillary also decreases the gas flow towards the vacuum chamber, and thus the vacuum pressure. In principle, this increases the maximum achievable capillary diameter.

2.3 Gas flow theory

In this section, the gas flow theory required for understanding the flows in the system described in section 2.2 will be discussed.

2.3.1 Flow rate

In order to minimize the pressure inside the vacuum chamber (for minimizing the absorption of XUV light, as described in section 2.2), the amount of gas flowing from the capillary into the vacuum chamber has to be minimized. This *flow rate* or *throughput*, can be expressed in units of $mbarLs^{-1}$ when dealing with a compressible flow.

To understand this, consider a tank with a relatively high pressure from which the contained fluid is gradually flowing out through a small opening. In the case of an *incompressible* flow, for example water, the flow would of course be equal to the time derivative of the volume of the fluid inside the tank. In the case of a *compressible* flow, however, the volume is held constant by the tank, and the pressure decreases. According to Boyle's law (pV = constant), the flow out of the gas tank is then equal to the time derivative of the product of gas pressure and tank volume and thus has units of pressure multiplied by volume per time. In this way, the *particle flow rate* q is defined, which is equal to the product of *volumetric flow rate* Q (Ls^{-1}) and pressure.

The gas flow through a tube, in the case of a laminar flow, restricted by the *flow conductivity* C of the tube, which is given by:

$$C = \frac{\pi D^4}{256 \mu L} p_{\text{high}}, \tag{2.6}$$

in which μ is the dynamic viscosity of the gas, L is the length, D the internal diameter of the capillary and p_{high} is the pressure in the tank (see appendix A for the complete derivation of this relation). Since the flow rate scales with the flow conductivity ($Q = C\Delta p$, in which Δp is the pressure difference across the tube), the (volumetric) flow rate also increases with the fourth power of the diameter: [6]

$$q = \frac{\pi D^4}{256 \mu L} p_{\text{high}}^2. \tag{2.7}$$

Since the gas inside the vacuum chamber would once again limit the output of the HHG setup by absorption, a method for keeping the pressure inside the vacuum chamber as low as possible (lower than 10^{-4} mbar) has to be developed. In other words, the particle flow rate q through the capillary into the vacuum chamber has to be limited.

This particle flow rate is what should be minimized, and not the volumetric flow rate, since the density of particles influences the absorbtion of the XUV light, but the speed at which the gas flows is of no importance for this process.

As follows from equation 2.7, it would theoretically be possible to increase the length of the capillary (as measured from the output slits to the entrance of the vacuum chamber), but it turns out that the length would have to be increased by unrealistically high values.

2.3.2 Pumping speed

The pumping speed indicates the amount of gas a pump can pump away per unit time. It is defined as the volume flow at the input of the pump, and thus has units volume per time. In this report, the symbol S and the units L/s (liters per second) are used for pumping speed.

Because the particle flow rate is $q = d(pV)/dt$, effectively meaning pressure times volumetric flow rate, the flow rate pumped out by a pump with pumping speed S at a pressure p can be expressed by (according to [5]):

$$q = p_{\text{pump}} S_{\text{pump}}. \tag{2.8}$$

However, this pressure is the pressure at the inlet of the pump. If the pressure at a chamber connected indirectly to a pump is known (in practice, the pressure at the gauge will always be different from the pressure at the pump), the flow rate pumped away from that point can be calculated as well, but then the local pressure should be multiplied by the effective flowrate

$$q = p S_{\text{eff}}. \tag{2.9}$$

The effective pumping speed can be calculated using the fact that the flow rate must be constant over the entire path, but can also be found experimentally, as explained in Appendix B. If pumping speed is referred to later in this report, the effective pumping speed will be meant, using the formula as $q = pS$.

2.3.3 Differential Pumping

Differential pumping is the technique of using different stages in a vacuum system, in which a large pressure difference has to be maintained between the first and the last section. The sections are typically separated from each other by flow restricting throttles. The advantage of this technique lies in the fact that the amount of gas pumped away by a vacuum pump increases with the gas pressure (equation 2.9), so that a relatively large portion of the gas can be pumped away in the first sections, and the pressure difference between two adjacent sections is relatively low. In the last section, a much

lower pressure can be achieved than after one section, since the pump attached to this section has to pump away a relatively low portion of the gas.

The system depicted in figure 2.4 can be interpreted as a differential pumping system, where the first section is the capillary and the second section is the vacuum chamber. The two sections are connected by the length of the capillary between the last outlet slit and the capillary end, which acts as a throttle, as in figure 2.8.

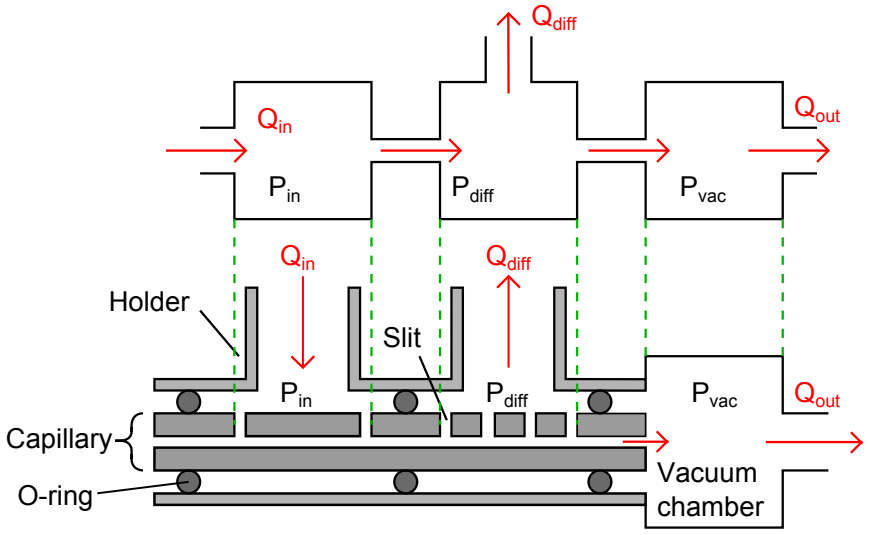

Figure 2.8: *Longitudinal cross section of the capillary system (schematic). The flows Q_{diff} and Q_{vac} are induced by vacuum pumps. The system can be devided into two sections in between which the pressure difference is significantly smaller than the pressure difference between the high pressure section in the capillary and the vacuum pressure, so that a low vacuum pressure can be maintained: in other words, differential pumping is used to achieve a low vacuum pressure.*

2.4 Gas flows in the system

To minimize the amount of gas flowing from the capillary into the vacuum chamber (see section 2.2), differential pumping (section 2.3.3) will be applied. To pump away the major part of the flow, extra orifices (where the first orifice is the open end of the capillary at the vacuum chamber) are created by cutting slits into the capillary wall, as shown in Figure 2.4. The gas flowing out of the slits is pumped away through a tube that is connected to a roughing pump[1]. Since the pressure at the outlet slits, inside the capillary, is relatively high, it is relatively easy to pump the gas out compared to pumping at the vacuum chamber. This is because, according to equation 2.9, the gas flow through the pump increases with the pressure, and thus more gas can be pumped away with the same pump if the gas pressure is high than if the gas pressure is low.

The gas pressure at both inlet slits of the capillary should be equal, which leads to a constant pressure level in the section between these two slits. The resulting pressure difference induces a gas flow through the capillary from the higher pressure section to the vacuum chamber. When differential pumping is applied, a significant part of this flow will be diverted through the outlet slits, such that only a small part will reach the vacuum chamber.

Simulations of the pressure and particle density profile inside a capillary were conducted by Edwin van der Weide[2] from Twente University. In figure 2.9, results of these simulations are shown. The top

[1] A roughing pump is any kind of vacuum pump used to initially evacuate a vacuum system; the term is derived from the range it works in: in a 'rough vacuum' the minimum achievable pressure is above 10^{-3} mbar.

[2] E.T.A. van der Weide, research group TS, University of Twente, e.t.a.vanderweide@ctw.utwente.nl

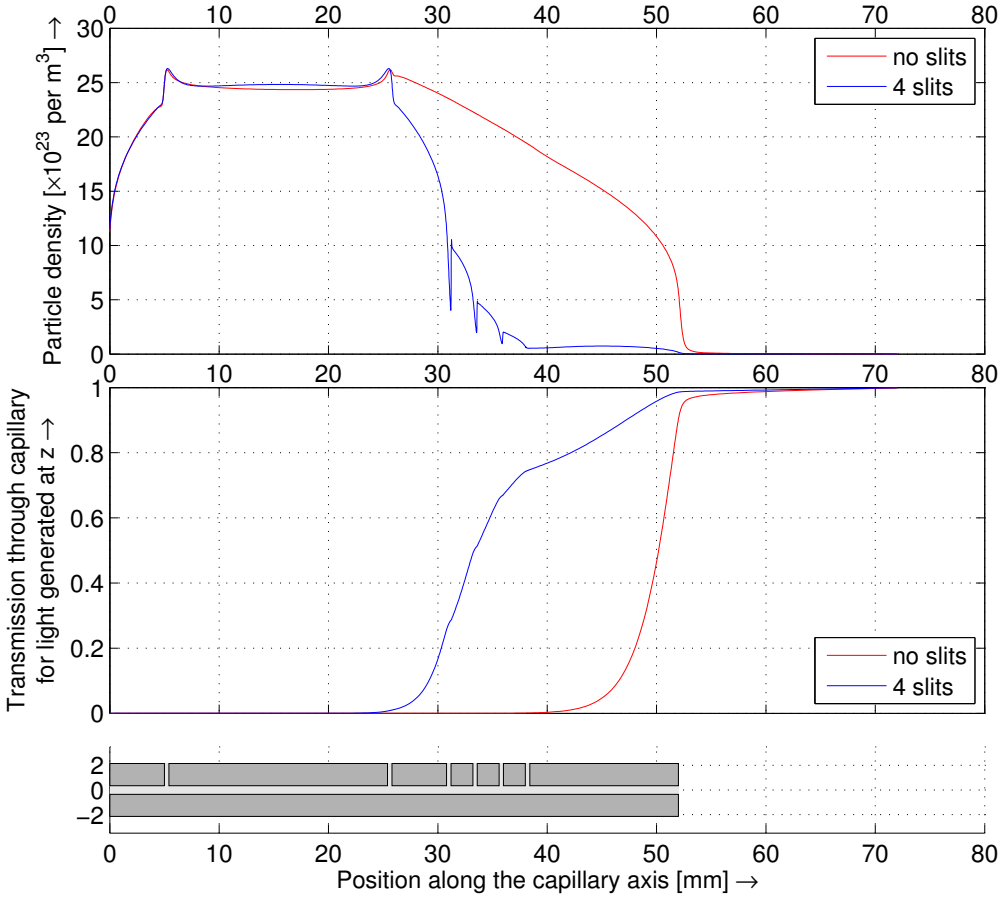

Figure 2.9: *The top plot shows the profile of the particle density along the optical axis in the capillary for two different situations: with no outlet slits and with four equally spaced outlet slits. The plot clearly shows a decrease in particle density in the section behind the active section when the slits are added. In the second plot, the transmission for light generated at a position z on the axis of the capillary is shown. In other words, the plot shows which fraction of the light generated at a certain position in the capillary actually comes out of the system. Blue lines represent the situation for the capillary shown below the plot, while the red lines represent the situation for a capillary of the same dimensions, without the 4 outlet slits. The data were taken from a computer simulation conducted by Edwin van der Weide. The reliability of the results for the particle density in the vacuum chamber (to the right) can be doubted.*

plot shows the profile of the particle density along the optical axis in the capillary for two different situations: with no outlet slits and with four equally spaced outlet slits. The plot shows a strong decrease in particle density in the section behind the active section when the slits are added. Since a high particle density leads to a high absorption of the high harmonic radiation (see section 2.2.2), this leads to a higher transmission of high harmonic radiation through the capillary. This is illustrated in the bottom plot of figure 2.9: it shows the normalized output intensity as a function of the position at which the light is generated. Without slits, only light generated at the end of the capillary is not fully absorbed. However, due to a large phase mismatch, there will be very little light generated in that part of the capillary. With slits, light generated around the second inlet slit will not be fully absorbed. Here the phase mismatch is not that large, so this part of the capillary will be the main contributor to

the total high harmonics output. This is conform to literature [2]. Concluding, figure 2.9 shows that outlet slits have a strong beneficial effect on the high harmonics output intensity.

Figure 2.10 gives a different view on the calculated absorption of generated light. It shows four curves representing absorption during the propagation of light generated at a certain point in the capillary. In those curves the Lambert-Beer relation (equation 2.5) can be recognised: the intensity drops exponentially. Solid lines show the propagation of light through a capillary with 4 outlet slits, while dotted line show propagation through a capillary without outlet slits. The red lines show that light generated at the beginning of the active section is fully absorbed regardless of the amount of slits. This is evident, because the pressure between the inlet slits is kept constant at a high pressure. The green and blue lines show that in the capillary with slits, light generated at the end of, and just after the active section is transmitted, although a large part is still absorbed (transmission up to 25%), while in the capillary without outlet slits all light is absorbed. The purple lines show that absorption behind the capillary is neglectable.

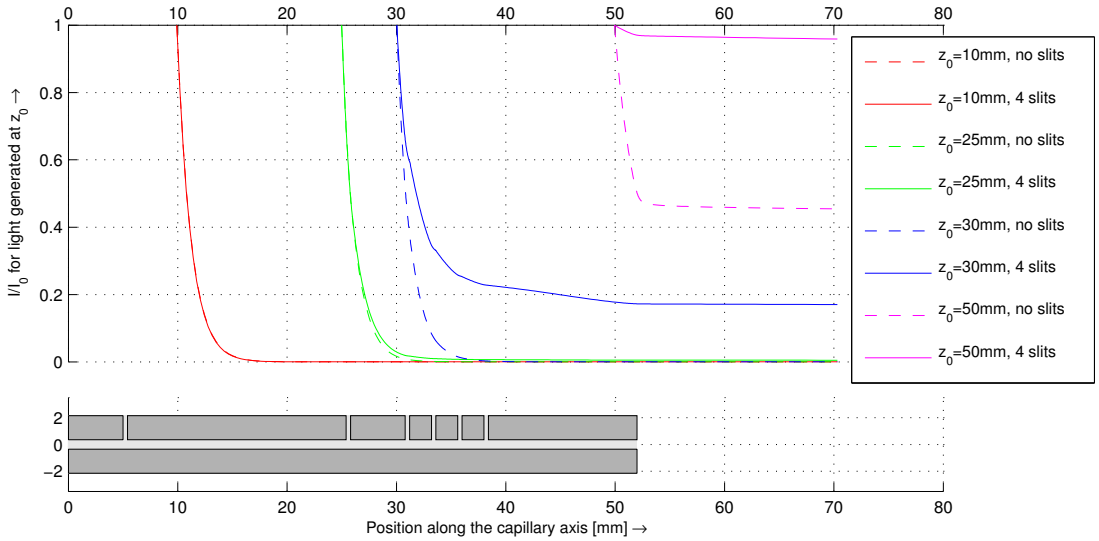

Figure 2.10: *This plot shows how the intensity of light generated at a certain position z_0 on the capillary axis changes when propagating through the capillary and vacuum chamber. Solid lines represent the situation for the capillary shown below the plot, while the dashed lines represent the situation for a capillary of the same dimensions, without the 4 outlet slits.*

Chapter 3

Experimental setup

In this chapter, the experimental setup for measuring the flow through a capillary waveguide and the end pressures achievable with the differential pumping system are described. Two types of experiments are carried out and described in detail.

In the first experiment, the relation between the flow through a capillary and the pressure difference across it is investigated for various capillary diameters and lengths. The experiment is conducted to acquire general knowledge on the flow through capillaries of this diameter. Also, the results will be used later to interpret the measurements from the second experiment. For the second experiment, the differential pumping setup as described in figure 2.8 is built. For various differential pumping configurations of the capillary, the pressure that can be achieved in the vacuum chamber is investigated as a function of the pressure at the capillary inlets. With this experiment, it can be shown that the maximum tolerable pressure in the vacuum chamber limits the diameter of the capillary that can be used in the high harmonic seed source.

3.1 Capillary flow measurements

To measure the flow through a capillary of certain length and internal diameter, the capillary is attached to a pressurized gas tank on one end and to a vacuum chamber on the other end. The pressure difference across the capillary induces a gas flow from the tank to the vacuum chamber. The flow rate of the gas can be determined from the change in pressure in the tank.

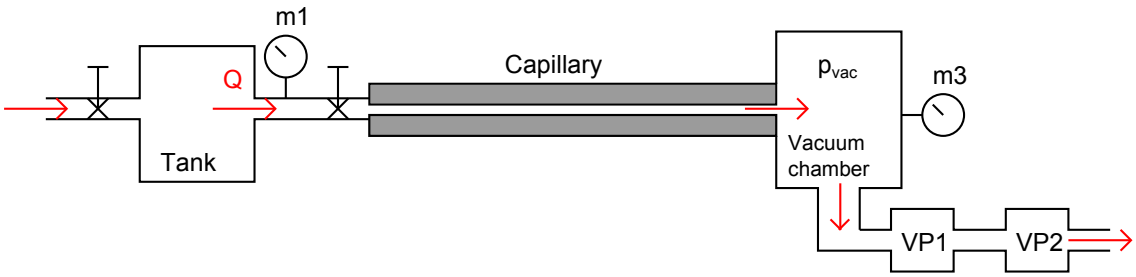

Figure 3.1: *Schematic of the setup used to measure the gas flow through capillaries of different lengths and internal diameters. VP1-VP3 indicate the pumps and m1-m3 indicate the pressure meters. VP1 is a turbomolecular pump; VP2 is a rotary vane pump. The effective pumping speed of VP1 and VP2 connected to the vacuum chamber was determined to be 38.4 L/s (see appendix B)*

The gas tank has a volume of 4.5 Liters and is filled with argon up to several hundred millibar of pressure. The tank is connected to one side of the capillary, as shown in Figure 3.1. Connected to the other side of the capillary is a vacuum chamber in which the pressure is kept below 10-3 mbar. When the valve between the gas tank and the capillary is opened, the gas starts flowing to the vacuum

chamber at a rate of $q = \frac{d(pV)}{dt}$ (see section 2.3.1). By measuring the pressure drop in the tank, with meter m1, the flow rate can be determined using the relation $q = V_{tank}\frac{dp}{dt}$. This experiment is conducted for different capillary lengths and diameters in order to determine the influence of those parameters on the flow rate. The pressure inside the vacuum chamber is continuously monitored to check if it does not rise too much. This is neccesary, because it is assumed that the vacuum pressure is negligible, so that the pressure drop over the capillary is equal to the pressure in front of it.

The pressure in the gasbottle is measured with a barocel pressure sensor (Edwards type 600ab, connected to a Datametrics 1500 readout) denoted in figure 3.1 as meter m1. The analog electrical output signal of the readout is connected to a National Instruments DAQmx Data Acquisition Card, which converts the analog signal into a digital signal. This digital signal is then processed and stored by a computer such that continuous measurements can be performed automatically over a period of time long enough for the pressure in the argon tank to reach a value well below the pressure required for HHG. Typically the measurements are stopped when a pressure of the order of 5 mbar is reached. The pressure in vacuum chamber is measured with a Penning-manometer connected to a Balzers TPG300 controller and denoted in figure 3.1 as meter m3.

3.2 Differential pumping measurements

For various differential pumping configurations of the capillary, the pressure that can be achieved in the vacuum chamber is investigated as a function of the pressure at the capillary inlets. For this the setup shown in figure 3.2 is used.

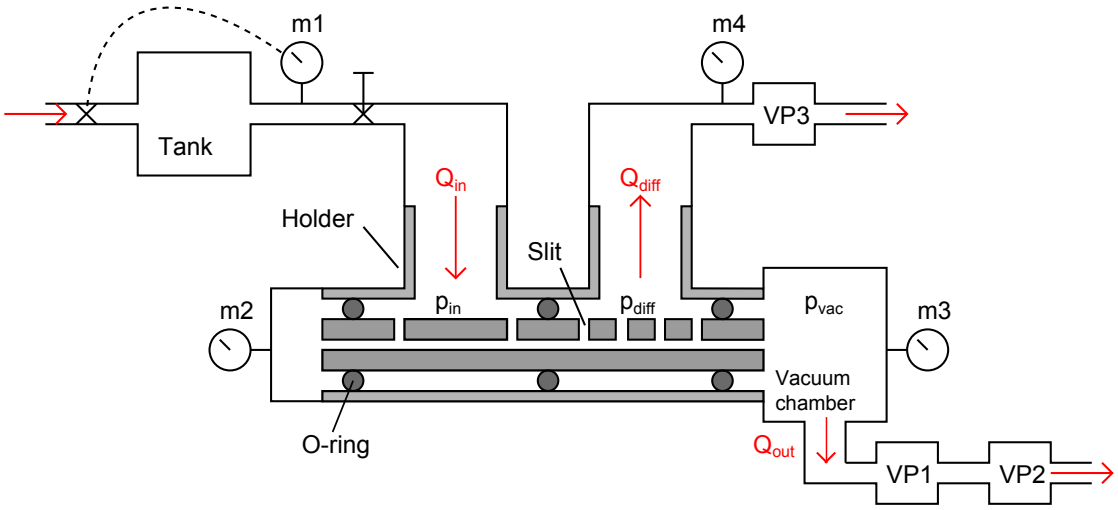

Figure 3.2: *Schematic of the setup used to measure the end pressure in the vacuum chamber for various configurations of the outlet slits implemented for the differential pumping of the capillary. VP1-VP3 indicate the pumps and m1-m4 indicate the pressure meters. The red arrows indicate the gas flows. The effective pumping speed of VP3 connected to the outlet tube of the capillary holder was determined to be 5.8 L/s (see appendix B).*

In the experiment, a specific pressure p_{cap} is set at the inlet slits after which the system is allowed to establish an equilibrium in pressure. When equilibrium is reached, a next value for p_{cap} is set, and so on, until the pressure in the vacuum chamber is measured for a broad range of inlet pressures. The pressure in the capillary is set by a PID regulator that controls the gas flow out of the argon tank using the feedback from a pressure meter at the capillary (m2 in figure 3.2). The reference value for the PID regulator is provided by a LabView VI, which automatically performs a programmable series of measurements at different pressures and maintains each pressure value long enough to make sure

that the system is in equilibrium (i.e. all the measured pressures are constant for a certain time, like for example ten seconds). Per second, ten datapoints are stored. In this way, the value of p_{vac} corresponding to each value of p_{in} can be obtained by averaging over the last few seconds. A more detailed overview of this setup can be found in appendix C. Using the pressure data collected by the VI, the flow rates Q_{diff}, Q_{out} and Q_{in} can be calculated using $Q = pS_{\mathrm{eff}}$ (see Appendix B).

The measurements of the pressure in the differential pump section and the vacuum chamber are performed for capillaries with varying lengths and diameters, different numbers of output slits and different pump tube diameters for the differential pumping section. From such detailed measurements, we will be able to determine the lowest achievable pressure in the vacuum chamber as a function of the optimum inlet pressure required for efficient phase matched HHG (this inlet pressure depends on the capillary diameter).

Figure 3.3 shows a technical drawing of the general configuration of a capillary. The number of outlet slits, the inner diameter, the total length and thus the length from the last slit to the capillary end are varied. The width of the all the slits (0.4 mm) and the distances between the slits (20 mm between the inlet slits, 2 mm between to adjacent outlet slits and 5 mm between the second inlet and the first outlet slit) are standardized and fixed. The length of the capillary from the last slit to the capillary exit is defined as the resistance length L_{res} and has the purpose to provide extra resistance for the gas flow towards the vacuum chamber.

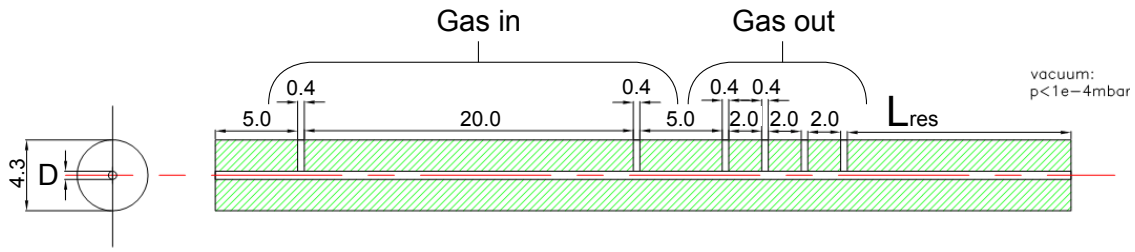

Figure 3.3: *General configuration of a waveguide capillary with integrated outlet slits for differential pumping. The widths of the inlet and outlet slits, as well as the distances between the slits are fixed. The resistance length L_{res}, the inner diameter D and the number of outlet slits are varied. The right side of the capillary is connected to the vacuum chamber. All dimensions are given in mm.*

3.3 Accuracy of measurements

There are two different types of measurement errors that can affect the accuracy of performed measurements: statistical errors and systematical errors.

In the capillary flow measurements, the statistical error manifests itself in the (relatively low) noise in the measured signal. In order to calculate the flow, however, the time-derivative of the measured signal has to be taken (see section 2.3.1). This time-derivative cannot be calculated numerically, because the noise is amplified strongly by differentiation[1] (see figure 3.4a). To solve this problem, a highly accurate polynomial fit to the data was made from which an algebraic derivative is taken (see 3.4b). The deviation between the original signal and the polynomial fit is very small and negligible relative to the absolute value of the signal.

In the differential pumping measurements, ten datapoints were stored every second for all the measured pressures (see appendix C), so that statistical errors can be virtually eliminated by taking the average value of multiple points, which was done in the differential pumping measurements. The actual error bars in the figures are, in fact, too small to be visible.

[1]The numerical derivative with step size Δn, $\frac{dx}{dt}(n) = \frac{x(n)-x(n-\Delta n)}{t(n)-t(n-\Delta n)}$, gets very distorted when used on a noisy signal because $x(n)$ might have a value that is very different from $x(n-\Delta n)$ due to noise, so that $x(n)-x(n-\Delta n)$ is not according to the shape of $x(t)$.

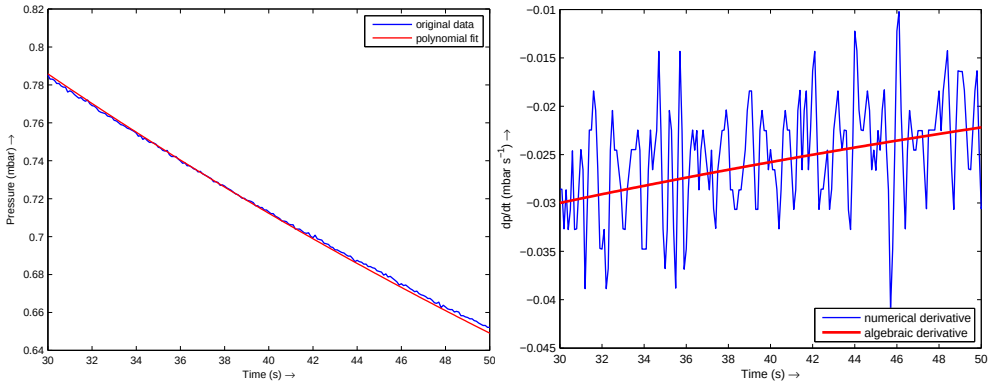

(a) **(b)**

Figure 3.4: *a) Plot of the signal from a pressure sensor and of the polynomial fit to this signal, b) numerical calculation of the time derivative from the pressure signal leads to a large increase in noise, while an algebraic derivative from the polynomial fit yields a smooth curve.*

Systematical errors, of course, are a lot harder to deal with. Measurements that are taken over a 4-second period, during which the whole system is in pressure equilibrium, can still not be completely accurate because of, for example, a gas leak somewhere in the system. Another factor which might have caused measurement inaccuracies is the fact that in some differential pumping experiments, tape was used to close the last slits of a capillary. This was done so that only one capillary had to be fabricated, while still measurements at different numbers of slits could be performed. If the taping was not entirely gastight, this would give rise to a systematical error.

Chapter 4

Results

In this chapter, the measurements that are performed on the flow in capillaries and the differential pumping of capillary waveguides will be discussed. In the first section of this chapter, data will be presented that are obtained from the measurements on the gas flow through capillaries of different length and inner diameter. In the last section, the measurements on the vacuum pressure will be presented for capillary waveguides with an integrated differential pumping section. For the experiments, we used the experimental setups described in chapter 3.

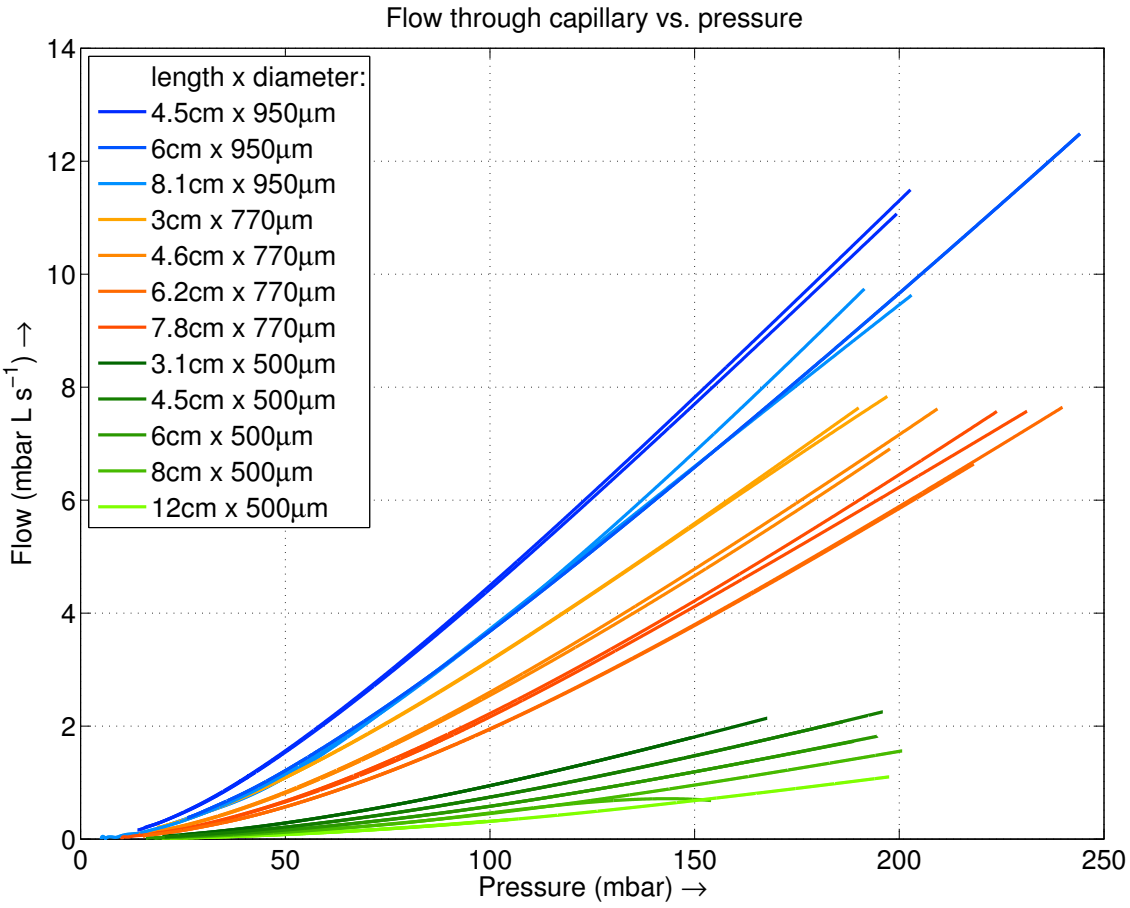

Figure 4.1: *Plot of the flow rate versus pressure difference for capillaries with three different inner diameters and of various lengths. Output tube diameter = 7 mm.*

4.1 Capillary flow measurements

Flow measurements are performed to get a detailed understanding of the gas flow through the capillaries used in a later stage for differential pumping. These measurements allow us also to calculate the pumping speeds of the vacuum pumps that are used. Information on the pumping speeds is required for processing the data from the experiments on differential pumping. By using the experimental setup discussed in section 3.1, the flow through various capillaries is determined as a function of the pressure difference over the capillary, for three different capillary diameters and different lengths. For this purpose, the pressure difference over the capillary has been measured as a function of time. The flow rate is then calculated from the time derivative of the pressure multiplied with the volume of tank as given by the equation $q = V_{tank}\frac{dp}{dt}$ (see section 2.3.1). Figure 4.1 shows a graph of the flow through the capillaries as a function of the pressure. From the graph it can be seen that the flow increases with the pressure difference across the capillary. Decreasing the length of the capillary leads to an increase of the flow rate. However, the influence of the length on the flow rate is much less significant than the influence of the capillary diameter, which is well visible in the graph. If the diameter is increased approximately by a factor of two, from 500 μm to 950 μm, the flow increases by nearly a factor of five. Yet, if the length of the capillary is halved, from 8.1 cm to 4.5 cm, the flow increases only by less than a factor of two. A further analysis of the data of figure 4.1 allows us to determine the flow regime of the gas flow through the capillary waveguides.

4.1.1 Flow regime

The curves for the flow rate versus pressure difference presented in figure 4.1 can be used to determine whether the gas flow in the capillary behaves as a laminar, viscous flow, like discussed in section 2.3.1. For this purpose, all the curves have been plotted on a double logarithmic scale in figure 4.2. In addition, also the theoretical flow rates for the capillaries with the highest and the lowest flow conductivity are calculated, using equation 2.7, and plotted in the graph. The capillary with the highest conductivity has a length of 4.5 cm and an inner diameter of 950 μm, and the one with the lowest conductivity has a length of 12 cm and an inner diameter of 500 μm.

Figure 4.2 shows that the theoretical flow curve for the capillary with the lowest conductivity (12 cm length, inner diameter 500 μm) fits very well to the measured flow, indicating that a laminar flow has established in the capillary. However, for the capillary with the highest conductivity (length 4.5 cm, inner diameter 950 μm) the measured flow is smaller than the theoretical flow. The graph shows that the flow becomes increasingly limited with increasing pressure.

To explain the deviation between the measured and theoretical flow, two effects that limit the in- and outflow of gas at the respective capillary ends have to be taken into account. Depending on the diameter, the flow needs a certain length to develop into a laminar flow, as shown schematically in 4.3.

The developing region increases in length for larger capillary diameters [7]. The longer this region is, the more it limits the flow through the capillary. This is in agreement with the data displayed in figure 4.4, which shows that for a fixed inner diameter, the shortest capillaries show the strongest deviation in flow with respect to theory. The influence of the developing region on the flow is the largest for capillaries with a large aspect ratio (ratio of diameter D and length L), and therefore have a high conductivity.

Next to a limitation on the flow at the entrance of the capillary (high pressure side), there also exists a limitation on the flow at the exit of the capillary (vacuum side). At the exit, the flow may be choked because the flow speed is limited to the speed of sound, i.e. a Mach number of 1. According to [8], this occurs at a critical upstream-to-downstream pressure ratio which depends on the specific heat ratio γ of the gas:

$$\frac{p_{\text{high}}}{p_{\text{low}}} \geq \left(\frac{\gamma+1}{2}\right)^{\frac{\gamma}{\gamma-1}}. \tag{4.1}$$

For argon $\gamma = 1.66$, such that $\frac{p_{\text{high}}}{p_{\text{low}}} = 2.05$. In our experiments, the upstream pressure is orders of magnitude higher than the downstream pressure and therefore it can be assumed that the flow at the

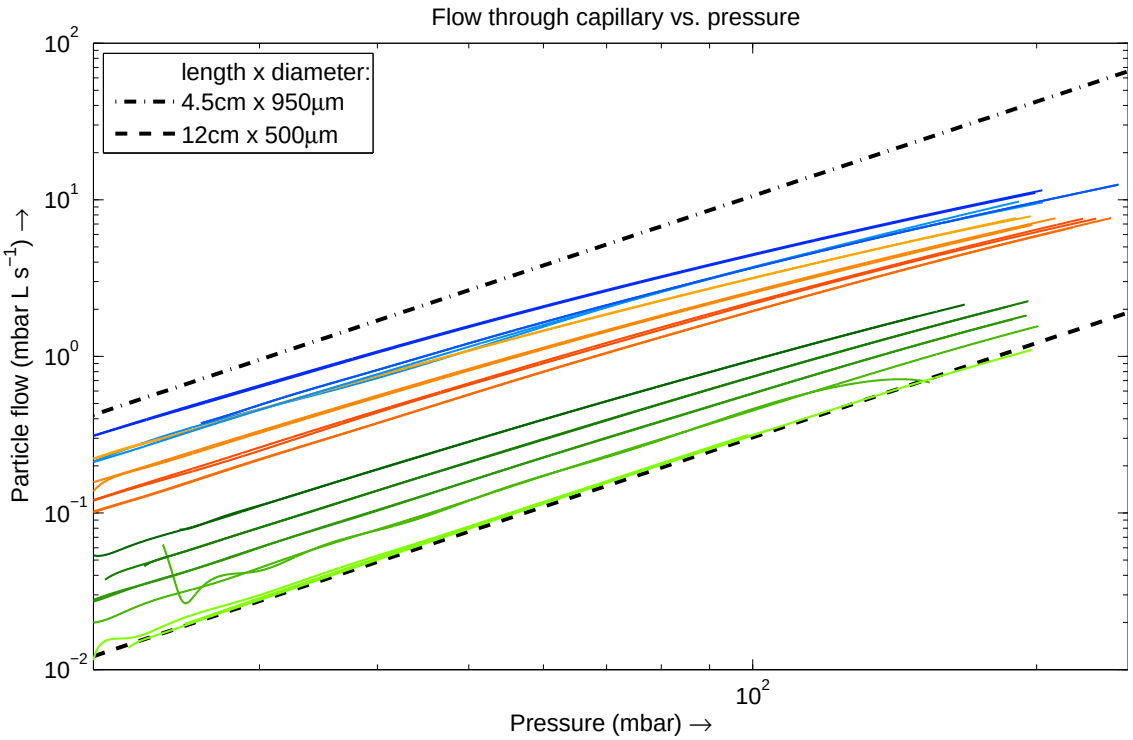

Figure 4.2: *Log-log-plot comprising the same curves as figure 4.1. The thick black lines are the theoretical values for the capillary corresponding to the upper curve (4.5 cm x 950 μm) and the lower curve (12 cm x 500 μm). The theoretical values have been computed using equation 2.7. Output tube diameter = 7 mm.*

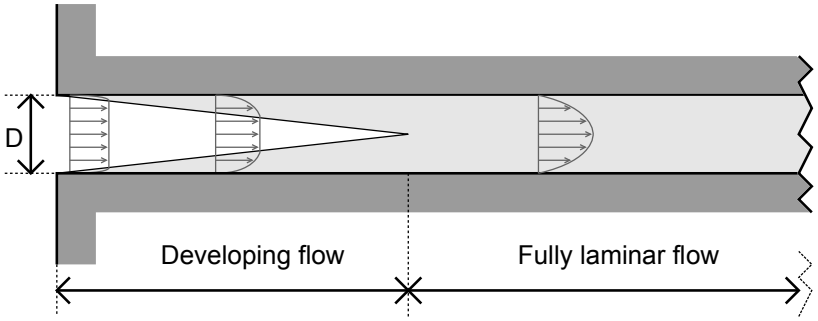

Figure 4.3: *Development of a laminar flow in a capillary. Only after a certain length, a laminar flow is established. This length increases with the diameter D, but is independent on the total length of the capillary. The white region indicates the region where the flow is not yet fully laminar.*

exit of the capillary is choked and limits the flow.

4.1.2 Influence of capillary length

Figure 4.4 provides a plot of the flow through capillaries with a fixed diameter of 500 μm versus the inverse of the capillary length for different pressures. The data were again taken from the same set as displayed in Figure 4.1. A linear graph is expected, since equation 2.7 features an inverse linear dependence on the capillary length.

The deviations from this linear dependence, apparent in 4.4, can be explained by the influence of the developing region at the entrance of the capillary where the flow is not fully developed or by the flow being choked at the end of the capillary, as explained in section 4.1.1. Both effects should have larger influence in shorter capillaries. Therefore, weighted linear fits are applied to the plots in figure 4.4, where the data points from longer capillaries have higher weights. Those fits indicate a good linear dependance for longer capillaries, while for very short capillaries, the measurements deviate quite strongly from the theory.

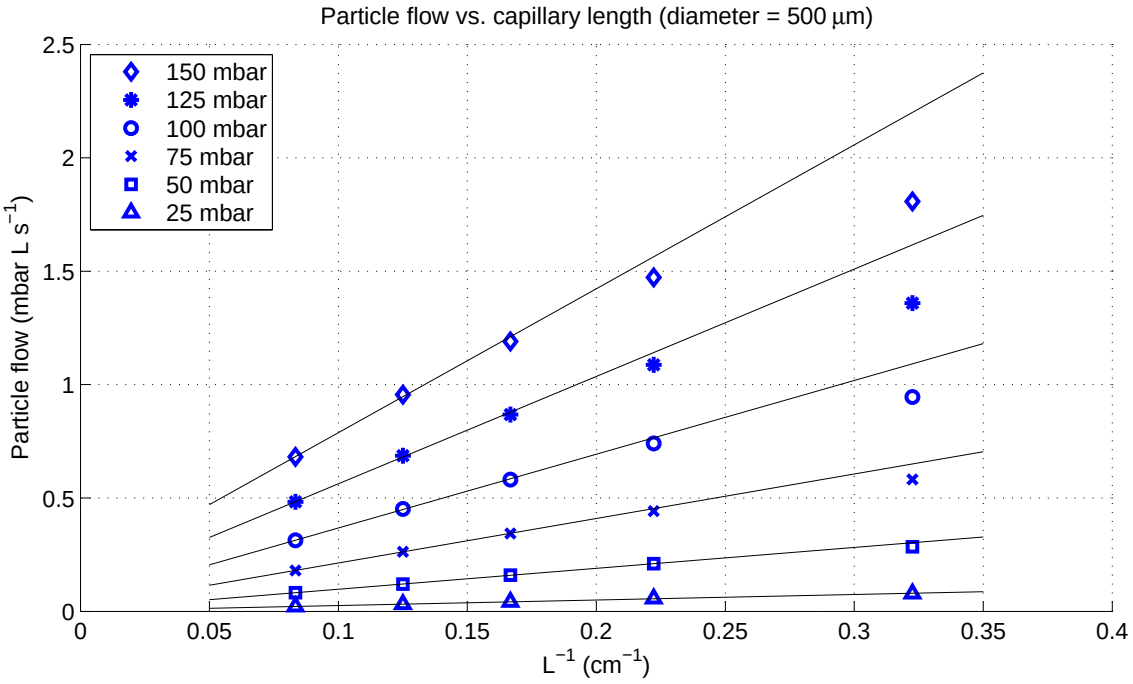

Figure 4.4: *Plot of flow rate versus the inverse of the capillary length for different pressures. Capillary diameter = 500 μm; output tube diameter = 7 mm. The black lines in the figure are linear fits. Higher flow values were given lower weights.*

4.1.3 Influence of capillary diameter

In figure 4.5, plots of the flow rate through the capillary versus capillary diameter are shown for different pressures. From the plots, we see that the flow increases nearly linear with the diameter of the capillary (the lines in the graph are a guide to the eye). The plot also shows that the pressure has a negligible influence on the dependence of the flow on capillary diameter. In contrast to the linear dependence of flow on capillary diameter, we expect from equation 2.7, which describes a laminar flow, that the flow increases with a fourth power of the diameter. The deviation between the measured flow and the flow calculated from laminar flow theory is attributed to the development of the flow at the entrance of the capillary and the choking of the flow at the exit of the capillary.

4.2 Differential pumping measurements

Using a setup specially built for differential pumping of the capillary waveguides, a series of experiments is carried out in which the pressure in the vacuum chamber is measured as a function of the pressure applied at the inlet slits of a capillary, for different capillary configurations including different capillary diameters, number of slits and residual lengths (distance from the last outlet slit to the end of the

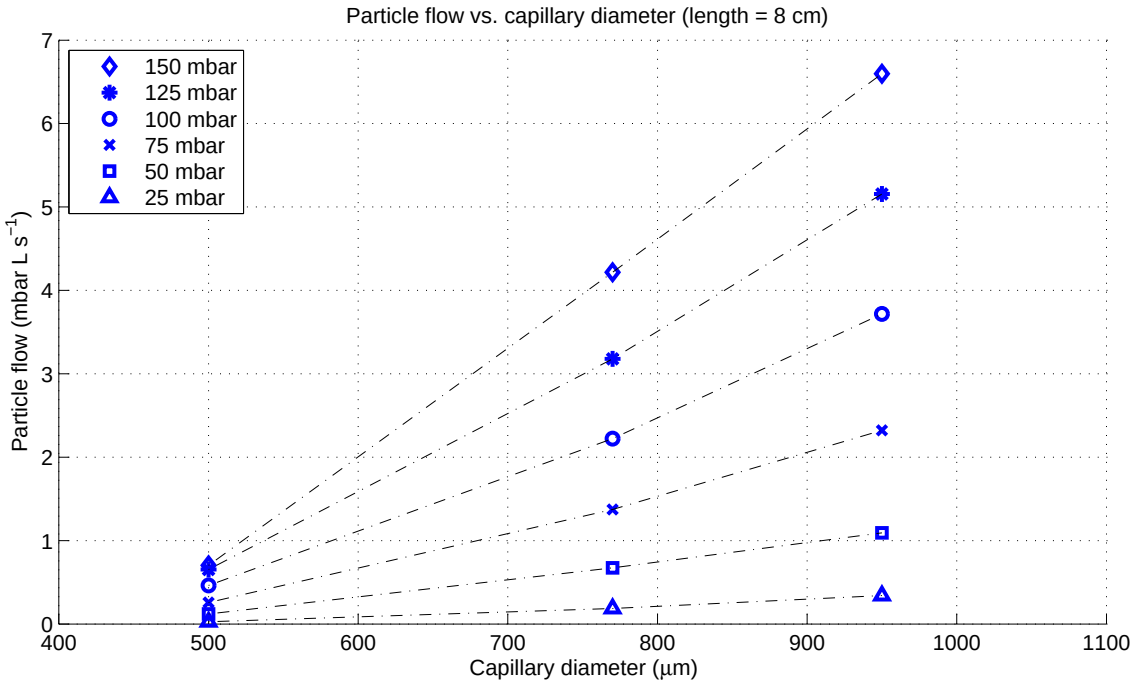

Figure 4.5: *Plot of flow rate versus capillary diameter for different pressures. Capillary length = 8 cm; output tube diameter = 7 mm.*

capillary, see figure 3.3). For this purpose, the different capillaries were placed inside a holder specifically designed for differential pumping (see section 3.2).

Figure 4.6 shows semi-logarithmic plots of the pressure in the vacuum chamber versus the pressure at the inlet slits of the capillary for various capillary configurations. A logarithmic scale is used here in order to make the order of magnitude of the vacuum pressure visible, which is more important than the exact value, since both absorption and flow change significantly over the large range of pressures obtained in the vacuum chamber.

From Fig 4.6a-d it can be seen that the vacuum pressure p_{vac} increases with the pressure p_{in} at the inlet slits, as one would expect. On a logarithmic scale, this dependency is approximately linear. The exact dependency of p_{vac} on p_{in}, however, differs per configuration.

For a capillary diameter of 150 μm, p_{vac} shows a different dependence on residual length and number of outlet slits, as depicted in figure 4.6a. If the length is decreased from 18 mm to 11 mm, while the number of slits is increased from 2 to 4, then figure p_{vac} decreases. Increasing the length further, up to 13.6 mm, while keeping number of slits fixed at 4, leads to a significant reduction of p_{vac}.

For larger capillary diameters, the dependence of the vacuum pressure on the inlet pressure for different residual lengths and number of outlet slits is similar. Figure 4.6b shows this for a capillary of 500 μm: an increase of the residual length leads to a decrease of p_{vac}, however, increasing the number of slits leads to a more significant decrease. Furthermore, a vacuum pressure of less than 10^{-4} mbar can be maintained for an inlet pressure of up to 100 mbar. This can be accomplished with a capillary with 6 slits and a residual length in the order of 10 mm. However, the number of slits also adds to the total length of the capillary and thus to the total absorption of harmonic radiation.

At a diameter of 770 μm (figure 4.6c), maintaining this vacuum pressure becomes more difficult. At a number of 10 slits and a residual length of 51 cm, $p_{\mathrm{vac}} = 10^{-4}$ mbar can only be maintained for inlet pressures of up to 50 mbar, while the capillary is relatively long.

At a diameter of 950 μm (figure 4.6d), it is virtually impossible to maintain a vacuum pressure of 10^{-4} mbar.

For a diameter of 770 μm (figure 4.6c), maintaining vacuum pressure as low as 10^{-4} mbar becomes

more difficult. For a number of 10 slits and a residual length of 51 mm, $p_{\mathrm{vac}} = 10^{-4}$ mbar can only be maintained for inlet pressures of up to 50 mbar, although the residual length is rather large. At a diameter of 950 μm (figure 4.6d), it is virtually impossible to maintain a vacuum pressure of 10^{-4} mbar.

Figures 4.6(a-d) show a general trend of increasing vacuum pressure for increasing capillary diameter. The number of slits and the residual length required for keeping the vacuum pressure low also increase with the diameter.

From the data presented in figure 4.6, it can be also concluded that the benefit of adding extra slits increases with the inlet pressure p_{in}. This can be derived from the slope of the p_{vac} vs. p_{in} curves: while these curves mostly lie in the same order of magnitude for low p_{in}, the values of p_{vac} begin to diverge as p_{in} increases. This means that the number of slits has a significantly larger influence at high inlet pressures than at low inlet pressures. This can be explained by the fact that the pressure decreases by a certain factor over each slit (see figure 2.9), so the absolute decrease in pressure depends on the inlet pressure.

4.2.1 Pressure in differential pumping section

Figure 4.7 shows a plot of the pressure in the differential section p_{diff} (see figure 2.8) versus the pressure at the inlet slits p_{in} for the same capillaries as are used in figure 4.6. The curves of p_{diff} vs. p_{in} for all capillaries are devided into four clusters, which correspond to the four different diameters that are used (150, 500, 770 and 950 μm). For figure 4.7, the values of p_{diff} have been averaged for all capillary configurations in each cluster. The standard deviation from this average value is depicted by the error bars.

The curves in figure 4.7 show an approximately linear dependence of p_{diff} on p_{in}. This implies that p_{diff} (and thus the flow q_{diff}) increases significantly with the capillary diameter, while the dependence on capillary length and number of slits are much less significant. In other words: the larger the diameter, the more gas will flow through the capillary and the more gas can be diverted, that is pumped away through the outlet slits. Although not visible in figure 4.7, the dependence of p_{diff} on p_{in} within each cluster is the strongest for the capillaries with the highest number of outlet slits. This is because the total conductance of the slits is higher, and therefore the flow and also the pressure in the differential pumping section are a somewhat higher.

The particle flow rates q_{diff} and q_{out} can be determined from the product of pressures and effective pumping speeds (see appendix B).

4.2.2 Influence of diameter of the outlet tube

In figure 4.8(a-d), the pressure in the vacuum chamber is plotted versus the pressure set at the inlet slits of the 500 μm capillary for two different diameters of the outlet tube connected at the differential section (see figure 3.2). The measurements are carried out for four capillary configurations with different numbers of outlet slits and residual lengths.

Figure 4.8a and 4.8b show that the diameter of the outlet tube has a significant influence on the vacuum pressure p_{vac}. For an outlet tube diameter of 3.5 mm, the graphs shows that the vacuum pressure that can be achieved with either four or six outlet slits in the capillary is similar. However, increasing the outlet tube diameter up to 7.0 mm, strongly reduces the rate at which the vacuum pressure increases with inlet pressure for a capillary with six outlet slits. At high inlet pressures, the final vacuum pressure that can be achieved lies around 10^{-4} mbar, which is almost a factor of four below the vacuum pressure that can reached with four inlet slits. Figure 4.8c and 4.8d show that if the diameter of the outlet tube is increased from 3.5 mm to 7.0 mm for a capillary with only one or two outlet slits, there is no significant change in vacuum pressure. So, the larger diameter outlet tubes appear to be much more significant for a reduction of the vacuum pressure for capillaries with a higher number of outlet slits. This means that the effect of increasing the number of outlet slits only has a significant effect up to a certain point, where the diameter of the outlet tube takes over as the limiting factor ('bottleneck') for the flow through the differential pumping section.

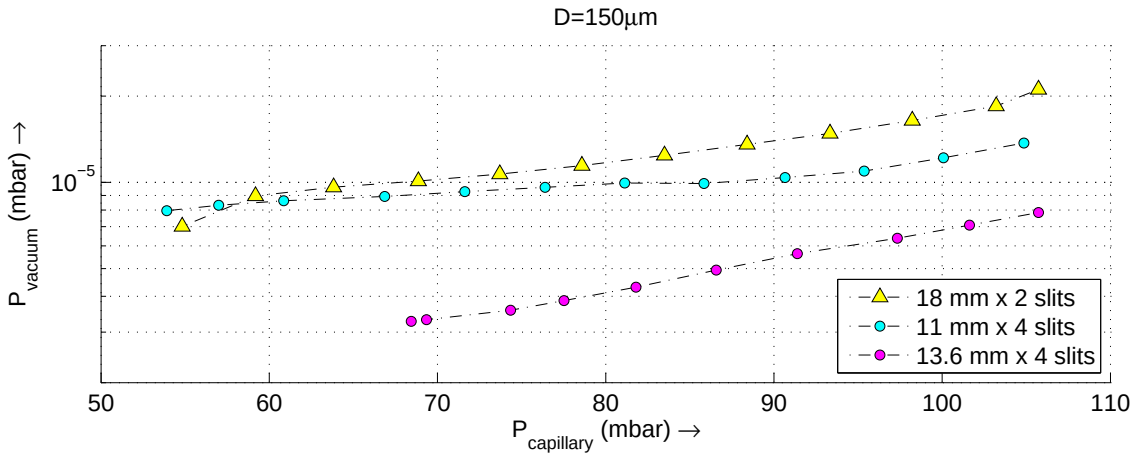

(a)

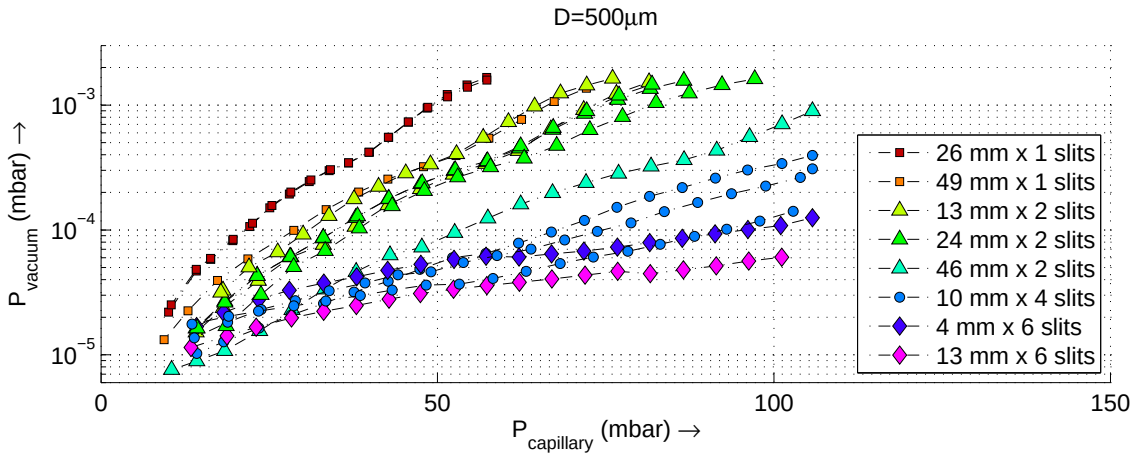

(b)

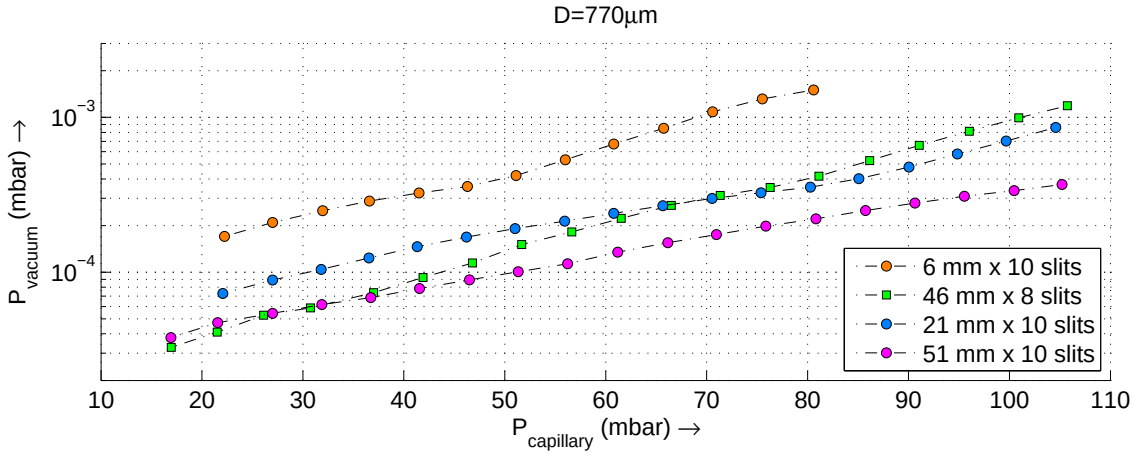

(c)

Figure 4.6: *(first three plots) Semi-logarithmic plots the pressure in the vacuum chamber as a function of the pressure at the inlet slits of the capillary for different capillary diameters, numbers of outlet slits and lengths from the last slit to the end of the capillary. The differential pumping outlet tube has a fixed diameter of 7.0 mm.*

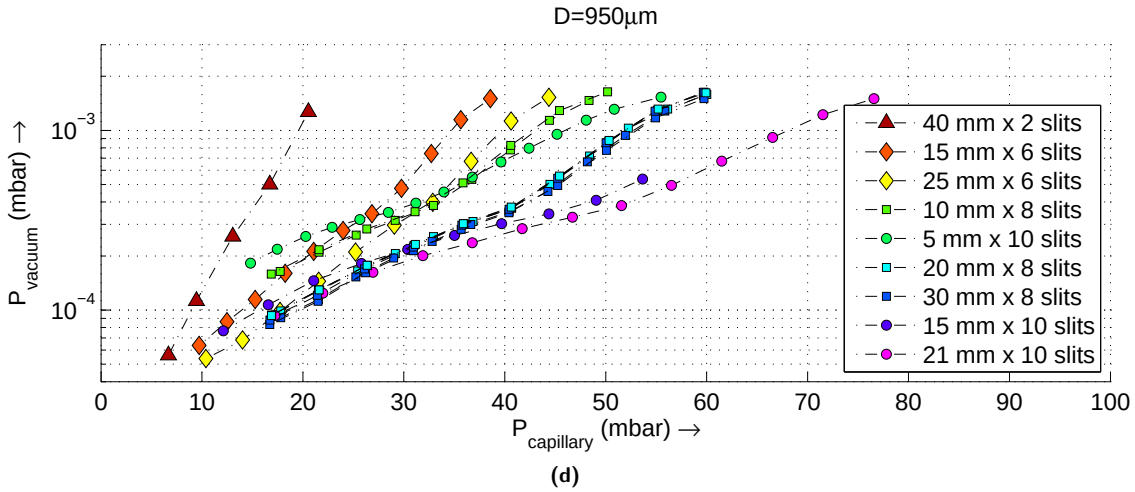

Figure 4.6: *(last plot) Semi-logarithmic plots the pressure in the vacuum chamber as a function of the pressure at the inlet slits of the capillary for different capillary diameters, numbers of outlet slits and lengths from the last slit to the end of the capillary. The differential pumping outlet tube has a fixed diameter of 7.0 mm.*

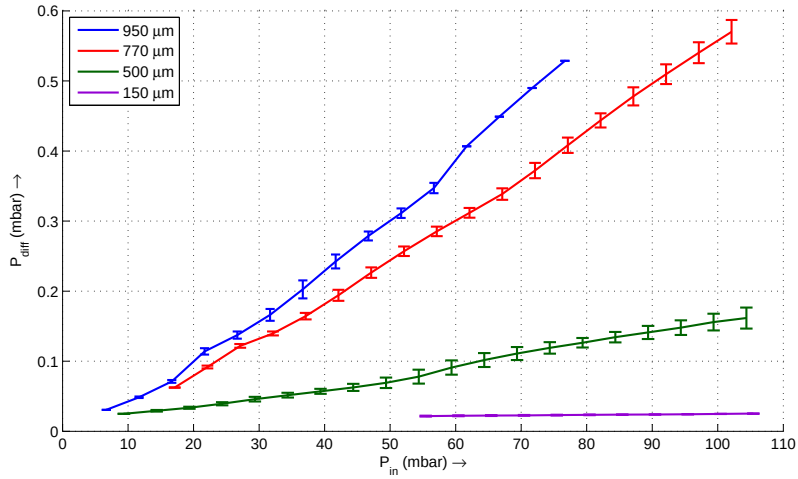

Figure 4.7: *Plot of the pressure in the differential pumping section p_{diff} versus the inlet pressure p_{in} for capillaries with 150, 500, 770 and 950 μm inner diameter. The data were obtained from the dataset used in figure 4.6. The plots show the averaged value of p_{diff} for the different capillary configurations (length and number of slits) used for each diameter. The error bars show the standard deviation.*

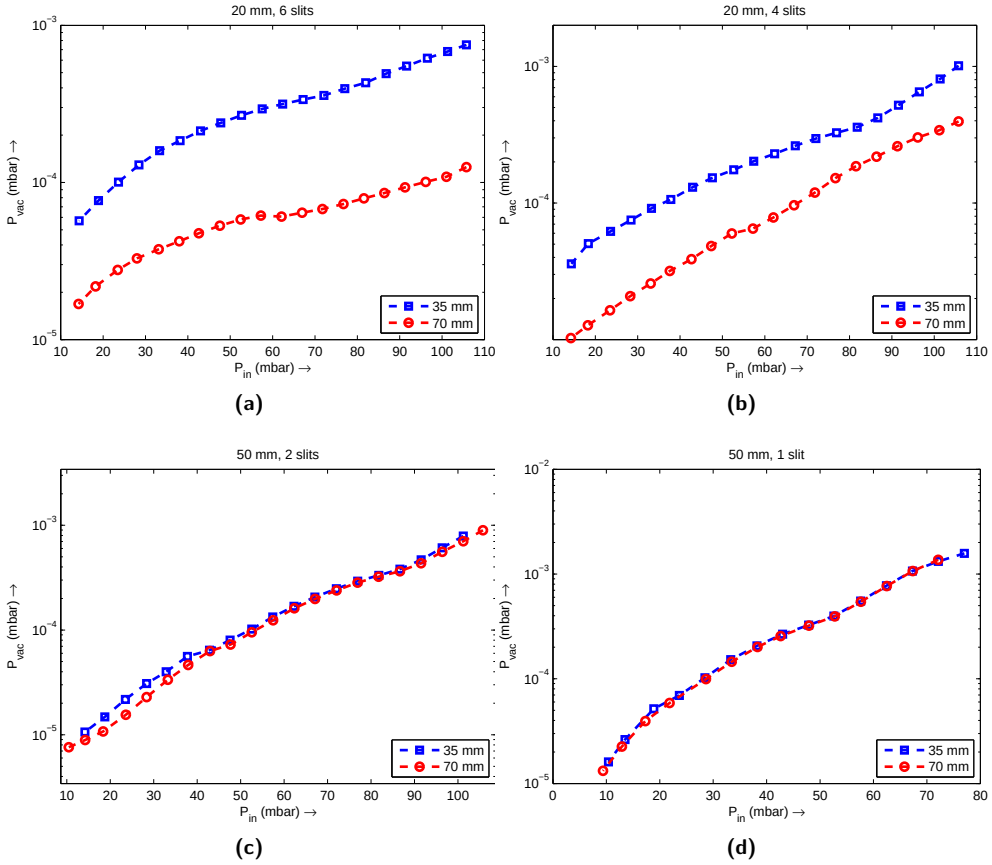

Figure 4.8: *Semi-logarithmic plots of the pressure in the vacuum chamber versus the pressure at the inlet slits of a capillary with 500 μm inner diameter for two different diameters of the outlet tube connected at the differential section. The diameter of the outlet tube was 3.5 mm and 7.0 mm, respectively.*

Chapter 5

Discussion and conclusion

This section will briefly summarize the conclusions that can be drawn from the data obtained in the experiments.

Measurements of the gas flow through capillaries with a small inner diameter and a long length, 500 m and 12 cm respectively, show that the (molecular) flow for pressures in the range between 1 and 200 mbar is laminar, where the flow rate can be described with Poiseuille's law (equation 2.7). However, for capillaries with a larger inner diameter and a shorter length the flow becomes limited in comparison to a laminar flow. This is caused by in- and outflow effects at both ends of the capillary. At the capillary entrance, the flow is smaller as it first has to develop into a laminar flow. At the exit, the flow becomes choked because the flow speed cannot exceed the sonic speed. Yet, this limitation on the flow by the capillary ends is in principle advantageous for the application considered in this report, since the goal is to increase the capillary diameter while limiting the flow.

From the measurements on the differential pumping of the capillary waveguides, we conclude that in order to keep the vacuum pressure low, while increasing the capillary diameter, the number of slits as well as the residual length (distance from the last outlet slit to the exit of the capillary) have to be increased. Doing so has the potential to decrease the flow into the vacuum chamber and thus the vacuum pressure by orders of magnitude. However, this does not necessarily mean that the total output power of high harmonic seed source will be increased. An important problem is that the residual length cannot be increased unlimited, because there still flows a certain amount of gas through this section of the capillary. This leads to a -compared to the vacuum chamber- relatively high pressure, which can induce a significant absorption of the high harmonics. For large residual lengths this effect may strongly reduce the total output power, so this effect should be considered when designing a capillary. More research will be required in order to find the optimal length, since no actual HHG experiments have been done in capillaries with a diameter of more than 150 μm.

To achieve phase matching in capillaries with larger inner diameter the pressure has to be tuned to a lower value which is advantageous if one wants to minimize the gas flow. A lower pressure leads to a lower gas flow into the vacuum chamber, which means that the residual length required to limit the flow as well as the pressure in the outlet section decrease. This in turn will lead to less absorption of harmonic radiation.

Our measurements on differential pumping show that the pressure in the vacuum chamber behind the capillary can be kept below a value of 10^{-4} mbar for capillary diameters ranging from 150 μm up to 950 μm. However, to stay below 10^{-4} mbar, the maximum pressure that can be applied in the active section decreases significantly for larger diameters, while the required residual length has to be increased significantly. It will thus be necessary to conduct high harmonic generation experiments, in which the output power of the high harmonics is measured, in order to find the best capillary configuration in terms of diameter, length and number of slits.

Chapter 6

Recommendations

In this chapter, we will try to give a few suggestions for further research. Included are possible ways for minimizing the vacuum pressure that we considered but were not able to investigate ourselves due to time issues.

6.1 High harmonic absorption measurements

In this research, we focused on keeping the vacuum pressure as low as possible for different capillary pressures, but what was not investigated is the actual required capillary pressure as a function of the diameter (see section 2.2.1). Since in capillaries with larger diameter, the theory presented in this section says that the required pressure is lower, the results presented in this report need to be interpreted while regarding this exact relationship. In other words, no exact quantitative conclusions can be drawn from these results about the maximum applicable capillary diameter (and thus laser beam energy) and optimum design. This presents a challenge for future research. Also, measurements on absorption have to be done, to find an optimum in residual length. Since absorption in the final section of the capillary is relatively high per length unit, leaving it shorter at the cost of a slightly higher vacuum pressure might lead to a higher yield of high harmonics. This has to be investigated.

6.2 Pulsed gas input

So far, we have only considered capillaries in which the pressure is kept constant. The pressure inside the capillary, however, does not necessarily need to stay at the level required for HHG. The TiSa drive laser will be operated at a repetition frequency of 50 Hz, synchronous with the Free Electron Laser. The required pressure only needs to be present at the time the drive laser pulse arrives at the capillary, in other words, the pressure could also be pulsed with a frequency of 50 Hz. This would of course reduce the total amount of gas flowing into the system and thus the pressure in the vacuum chamber. The question is, however, whether introducing a pulsed gas inlet is possible, since the pressure pulses would probably smooth out in the tubing connecting the argon tank to the capillary.

6.3 Periodic shutter

Using the same argument, one can argue that the capillary actually can be closed off from the vacuum tank, as long as the optical path is free at the time the high harmonic pulse will leave the capillary. This might for example be accomplished by placing a rotating shutter behind the capillary. In this way, gas would be leaking into the vacuum chamber only part of the time, which would make it easier for the vacuum pumps to keep up with the flow and keep the pressure low. The challenge here is of course to design a shutter which does not leak while closed.

6.4 Adding a second vacuum tank

To reduce the gas load on the Free Electron Laser further, it is be possible to connect a second vacuum tank behind the first one to conduct any high harmonic experiments in, and insert a flow restriction in between these two tanks, so gas can flow from the first tank to the second one only via a narrow opening (which would obviously have to lie in the laser beam's path). This way, it should be possible to bring the pressure inside the second vacuum tank down to a minimum. However, losses due to absorption in first chamber must be considered. In other words the pressure in the first chamber has to be pretty low already for this technique to be useful.

Bibliography

[1] The center for x-ray optics, November 2011.

[2] Christopher Andrew Froud. *Designing a Nanoscale X-ray Source: Towards Single Molecule X-ray Scattering*. PhD thesis, University of Southampton, 2007.

[3] C. Groot. Plasmon resonant bow-tie antennas for high harmonic generation. unpublished project report, February 2011.

[4] Jurjen Huisman. *Modelling of vacuum systems*. PhD thesis, University of Twente, 2006.

[5] L. Wolterbeek Muller. *Vacuümtechniek, Beginselen en toepassingen*, pages 140–145. Kluwer Technische Boeken B.V., 1989.

[6] Bruce R. Munson, Donald F. Young, Ted H. Okiishi, and Wade W. Huebsch. *Fundamentals of Fluid Mechanics*, chapter 8.2, pages 390–392. John Wiley & Sons, sixth edition, 2010.

[7] Bruce R. Munson, Donald F. Young, Ted H. Okiishi, and Wade W. Huebsch. *Fundamentals of Fluid Mechanics*. John Wiley & Sons, sixth edition edition, 2010.

[8] Donald J. Santeler. Exit loss in viscous tube flow. *J. Vac. Sci. Technol. A.*, 4(3):348–352, June 1986.

[9] E. Seres, J. Seres, and C. Spielmann. X-ray absorption spectroscopy in the kev range with laser generated high harmonic radiation. *Applied Physics Letters*, 89(18), 2006.

[10] Peter van der Slot. Free-electron lasers, from microwaves to x-rays. for Nederlands Centrum voor Laser Research (NCLR) B.V., 2004.

Appendix A

Derivation of the laminar flow rate

In order to derive the relationship between particle flowrate q and capillary diameter, we will first consider a cilinder of fluid inside a circular tube, and the forces acting on it, according to [6]. This situation is depicted in figure A.1.

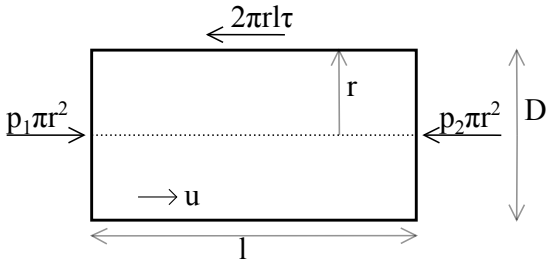

Figure A.1: *Schematic representation of a cylinder of fluid inside a (capillary) tube, with the forces acting on it.*

There are three different forces acting on this cylinder of fluid: two different pressure forces at the ends of the cylinder and the shear stress acting on the lateral sides. The force balance between these forces yields the following relation:

$$p_1 \pi r^2 - p_2 \pi r^2 - \tau 2\pi r l = 0 \tag{A.1}$$

where p_1 respectively p_2 are the pressures at either side of the cilinder of fluid, r is the tube radius ($= D/2$), l is the length of the cilinder, u is the flow velocity and τ is the shear stress.

If we define Δp as the difference between p_1 and p_2, this simplifies to

$$\frac{\Delta p}{l} = \frac{2\tau}{r} \tag{A.2}$$

Both the pressure difference and the capillary length, and thus the left side of this equation, are independent of the radial coordinate r. This means that the right side has to be independent of r as well, so the shear stress must be linearly dependent on r.

We know that the shear stress is zero at $r = 0$, and equal to the *wall shear stress* τ_w at $r = \frac{D}{2}$, so:

$$\tau = \frac{2\tau_w r}{D} \tag{A.3}$$

In other words, equation A.2 can be rewritten as:

$$\frac{\Delta p}{l} = \frac{4\tau_w}{D} \tag{A.4}$$

For a Newtonian fluid in a laminar flow, the following relationship holds for the shear stress:

$$\tau = -\mu \frac{du}{dr}, \tag{A.5}$$

where μ is the dynamic viscosity of the fluid. Using equation A.2, this can be rewritten as:

$$\frac{du}{dr} = -\frac{\tau}{\mu} = -\frac{\Delta p}{2\mu l} r \tag{A.6}$$

and this can be integrated to:

$$u(r) = -\frac{1}{2}\frac{\Delta_p}{2\mu l} r^2 + C_1 \tag{A.7}$$

in which C_1 is an integration constant. The value of this constant can be obtained using the no-slip condition, which means that the velocity at the cilinder walls is zero, so $u(\frac{D}{2}) = 0$, so

$$C_1 = \frac{1}{2}\frac{\Delta p}{2\mu l}\left(\frac{D}{2}\right)^2 = \frac{\Delta p}{16\mu l} D^2 \tag{A.8}$$

and

$$u(r) = \frac{\Delta p D^2}{16\mu l}\left[1 - \left(\frac{2r}{D}\right)^2\right] \tag{A.9}$$

The volumetric flowrate $Q = \frac{dV}{dt}$ through the tube or capillary is, by definition, equal to $\int u dA$, so it can be calculated as:

$$Q = \int_{r=0}^{D/2} u(r) 2\pi r dr = 2\pi \frac{\Delta p D^2}{16\mu l} \int_{r=0}^{D/2} \left[1 - \left(\frac{2r}{D}\right)^2\right] r dr \tag{A.10}$$

or

$$Q = \frac{\Delta p \pi D^4}{128\mu L}, \tag{A.11}$$

in other words, the flow rate *theoretically* increases with the fourth power of the diameter and with the inverse of the capillary length.

However, this equation only gives the *volume* flow rate Q. In order to obtain the *particle* flow rate q, or pV-flowrate, one has to multiply this by the pressure p:

$$q = \frac{\Delta p \pi D^4}{128\mu L} p \tag{A.12}$$

To find the total particle flow, this has to be integrated over the total capillary length (according to [4]):

$$q = \frac{\Delta p \pi D^4}{128\mu L} \int_{x=0}^{L} p(x) dx = \frac{\Delta p \pi D^4}{128\mu L} \int_{p_l ow}^{p_{\text{high}}} p dp \tag{A.13}$$

$$q = \frac{\Delta p \pi D^4}{128\mu L} \frac{1}{2}\left(p_{\text{high}}^2 - p_{\text{low}}^2\right) = \frac{\Delta p \pi D^4}{128\mu L}\left(\frac{1}{2}\left(p_{\text{high}} + p_{\text{low}}\right)\right)\left(p_{\text{high}} - p_{\text{low}}\right) \tag{A.14}$$

or

$$q = \frac{\pi D^4}{128\mu L} \bar{p} \Delta p. \tag{A.15}$$

If the assumption $p_{\text{low}} << p_{\text{high}}$ holds, however, this can be simplified to

$$q = \frac{\pi D^4}{256 \mu L} p_{\text{high}}^2 \tag{A.16}$$

since $\bar{p} \approx \frac{1}{2} p_{\text{high}}$ and $\Delta p \approx p_{\text{high}}$.

Since the flow conductivity C is defined as $C = \frac{q}{\Delta p}$, the flow conductivity of a capillary also scales with the pressure at the high pressure side of the capillary:

$$C = \frac{\pi D^4}{256 \mu L} p_{\text{high}}. \tag{A.17}$$

Appendix B

Measuring pumping speed and flow rate

In order to measure the pumping speed of our system, which is limited by the narrowest part of the connection between the vacuum chamber and the two pumps connected to it (see figure 3.1), we conducted a series of measurements in which we attempted to reach a constant pressure by filling the argon tank up to a pressure of 600 mbar and then adjusting the valve between the tank and the capillary. From these pressures and the corresponding flow rates (which could be obtained from earlier measurements, see for example figure 4.1), the pumping speed could then be obtained using the relation $q_{\text{out}} = p_{\text{vac}} S_{\text{vac}}$. Because we waited for the system to reach a state of equilibrium, $q_{\text{in}} = q_{\text{out}}$. The setup used for these measurements is depicted in figure B.1. A similar setup was used to measure the pumping speed of pump VP3 connected to the outlet tube of the capillary holder.

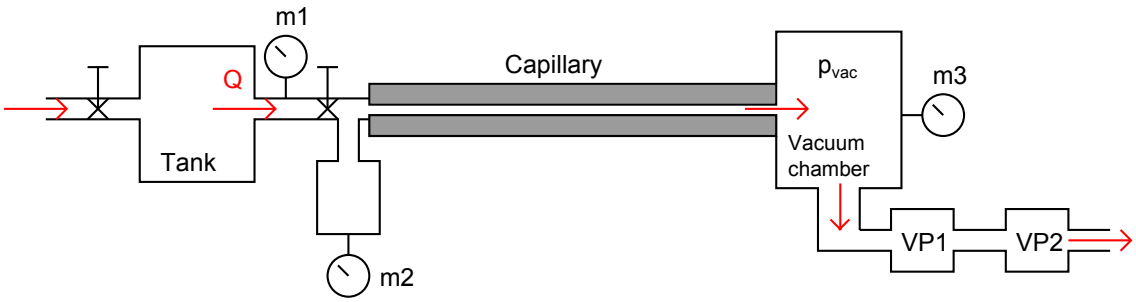

Figure B.1: *Schematic view of the setup used to measure the pumping speed of the setup.*

In this way, the pumping speed of pumps VP1 and VP2 connected to the vacuum chamber was determined to be 38.4 L/s, and the pumping speed of VP3 connected to the outlet of the capillary holder to be 5.8 L/s.

To determine the flow rate pumped out by differential pumping (q_{diff}), an experiment is conducted using the setup shown in figure 3.2. When the system is in equilibrium, the flow into the vacuum chamber is equal to the flow out of the vacuum chamber. Since the flow out of the vacuum chamber can be calculated using $q = pS$, the flow into the vacuum chamber(q_{vac}) can be calculated when the system is in equilibrium. The same holds for the chamber behind the output tube, so in a state of equilibrium, the flow out of the capillary via the output slits (q_{diff}) can also be determined.

Note that in this approach, the pumping speed is assumed to be independent of pressure. While this is not generally true, the used pumps have approximately constant pumping speeds at the pressure range in which the experiments discussed in this report were performed.

The pumpset VP1/VP2 comprises a turbomolecular pump (Pfeiffer, type TPH240-KGT, volume flow rate 210 L/s) and a roughing pump (Pfeiffer, type DUO 004B, volume flow rate 4 m3/h). The

vacuum pump VP3 is a roughing pump with a high pump capacity (Pfeiffer, type DUO 030A, volume flow rate 30 m^3/h).

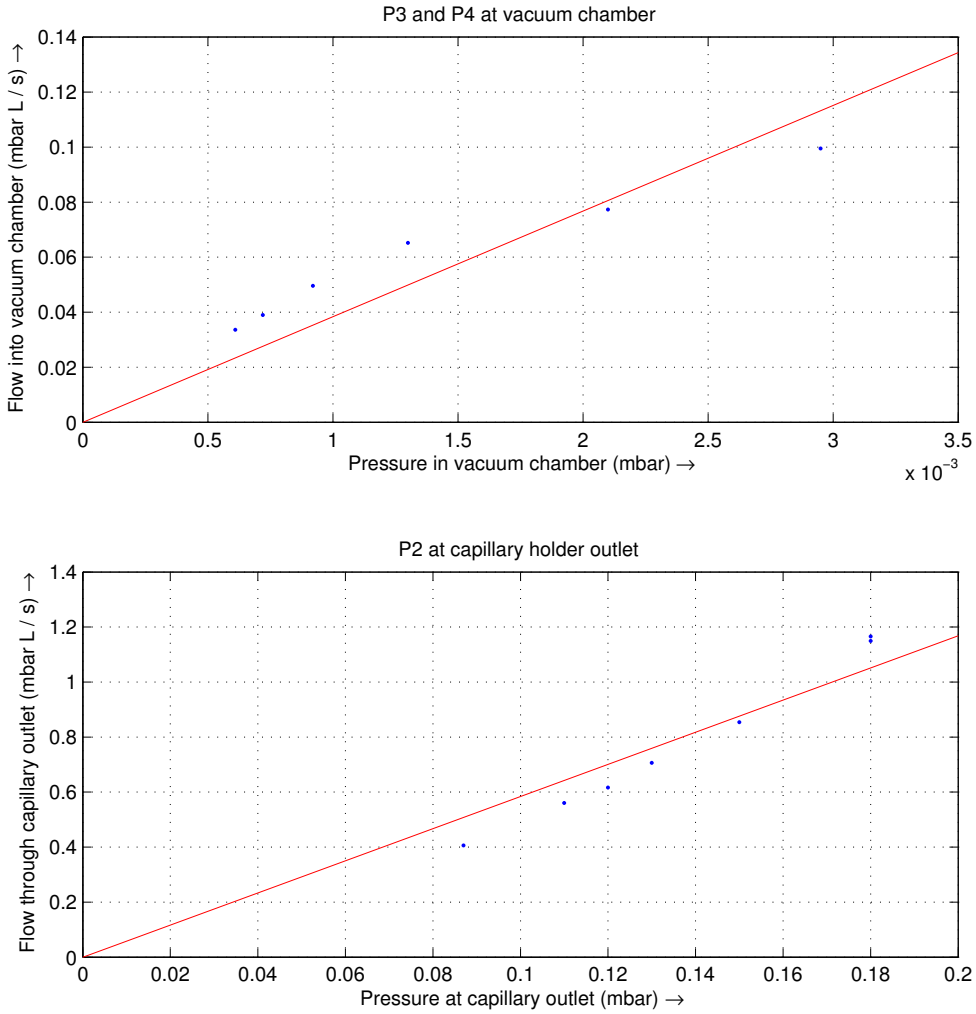

Figure B.2: *Measurements for the calculation of the pumping speed.*

Appendix C

Instrumentation

For measuring the pressures in different sections in the system simultaniously, while at the same time controlling the inlet pressure, the setup depicted in figure C.1 was used. The four different pressure meters all provide a certain output voltage, which is monitored by means of a National Instruments DAQmx data acquisition card at a rate of ten samples per second and stored in the memory of the attached computer, using a custom-made LabView VI (Virtual Instrument). This VI can be found in figure C.3.

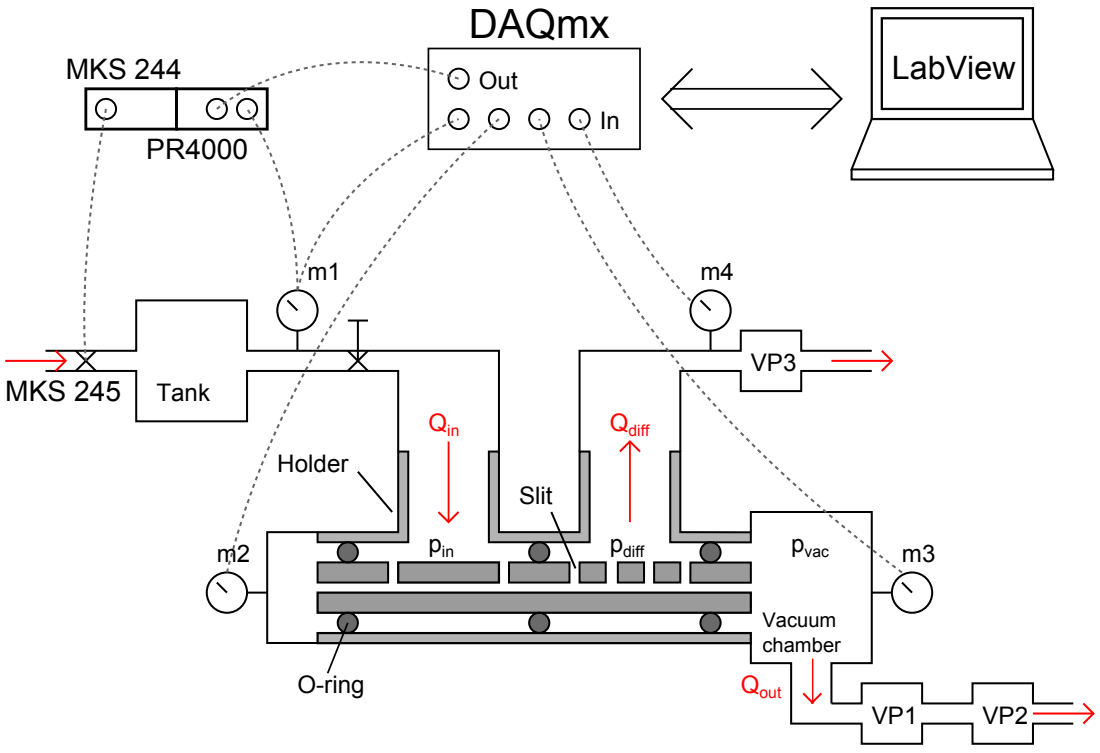

Figure C.1: *Schematic overview of the complete setup. The red arrows indicate the gas flows.*

In order to conduct measurements at different capillary pressures, a steady-state situation has to be reached, in other words, the pressures need to be held constant over a certain time. For this purpose an MKS Type 245 control valve is used, which is controlled by an MKS Type 244 Pressure/Flow Controller, which receives its information from a PR4000 power supply. This power supply uses the

pressure measured by sensor m1 to control the inlet valve, so that it holds the pressure inside the argon tank constant.

The PR4000 power supply receives the setpoint voltage (corresponding to the pressure value to be reached) via the DAQmx card from the computer, which uses the pressure inside the vacuum chamber (sensor m3) to ensure that the system has been in equilibrium long enough, with a default value of ten seconds. After these ten seconds the next setpoint is transmitted. A typical measurement series covers a range of 100 down to 10 mbar in 5 mbar intervals. Figure C.2 shows an example of the signals transmitted through the DAQmx card.

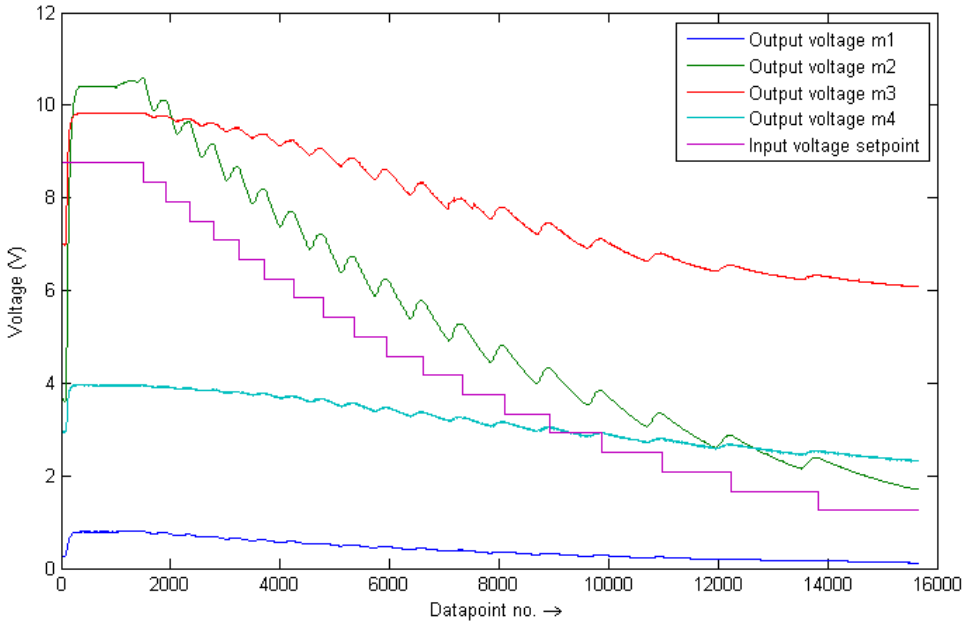

Figure C.2: *Input/Output voltages during a typical measurement series. Each pressure sensor has its own mbar-to-volt conversion, so the pressure scale is arbitrary.*

Figure C.3 shows the block diagram of the custom made LabView VI used for our measurements. The VI consists of one for-loop, which ensures that every second ten datapoints are stored. Inside the for-loop, a MatLab-script keeps comparing the last 50 datapoints (5 seconds) for the vacuum pressure to the 50 datapoints preceding these, and as soon as the differences in mean value and standard deviation between these two sets have crossed a certain threshold value, *and* the value of these datapoints is within a certain distance from the value that should be reached, the next setpoint voltage is transmitted. In this way, the VI ensures that for every setpoint, the system is in near-equilibrium for about ten seconds. In this way, the pressure value can be averaged over up to 100 datapoints per setpoint, which minimizes the statistical error.

A second MatLab script outside the for-loop saves all the datapoints in .csv-extension.

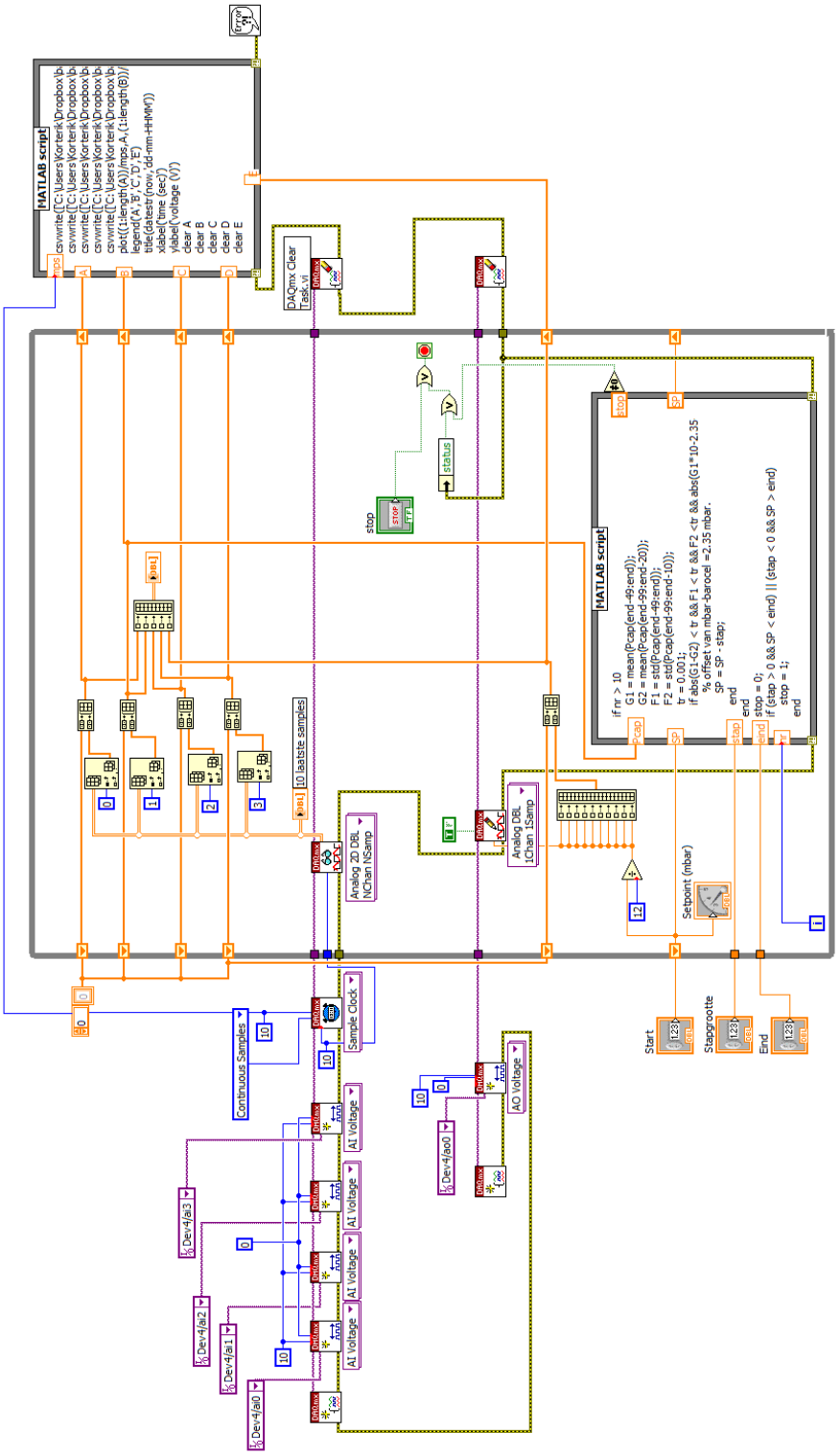

Figure C.3: *Block diagram of the LabView VI used in the measurements.*